



Stability of a realistic astrophysical pulsar and its mass-radius relation in higher-order curvature gravity

G. G. L. Nashed ^{1,*} and Kazuharu Bamba ^{2,†}

¹*Centre for Theoretical Physics, The British University,
P.O. Box 43, El Sherouk City, Cairo 11837, Egypt*

²*Faculty of Symbiotic Systems Science, Fukushima University, Fukushima 960-1296, Japan*
(Dated: July 8, 2024)

The objective of this research is to explore compact celestial objects while considering the framework of an extended gravitational theory known as $\mathcal{R} + f(\mathcal{G})$ gravity. The notations \mathcal{R} and \mathcal{G} denote the Ricci scalar and the Gauss-Bonnet invariant, respectively. Radio pulsars, which are neutron stars with masses greater than 1.8 times that of the Sun (M_{\odot}), provide exceptional opportunities for delving into fundamental physics in extraordinary environments unparalleled in the observable universe and surpassing the capabilities of experiments conducted on Earth. Through the utilization of both the linear and quadratic expressions of the function $f(\mathcal{G}) = \alpha_1 \mathcal{G}^2$, where α_1 (with dimensional units of $[length^6]$) are incorporated, we have achieved an accurate analytical solution for anisotropic perfect-fluid spheres in a state of hydrostatic equilibrium. By integrating the dimensional parameters α_1 and the compactness factor, defined as $C = \frac{2GM}{Rc^2}$, we showcase our capacity to encompass and depict all physical characteristics within the stellar structure. We illustrate that the model can produce a stable arrangement encompassing its physical and geometric properties. We illustrate that by utilizing the quadratic form of \mathcal{G} in the $\mathcal{R} + f(\mathcal{G})$ framework, the ansatz of Krori-Barua establishes connections between pressure in the radial direction (p_r) using semi-analytical methods, pressure in the tangential direction (p_t), and density (ρ). Remarkably, in the context of the positive/negative α_1 quadratic $\mathcal{R} + f(\mathcal{G})$ gravity framework, the maximum compactness is inherently restricted to values that fail below the Buchdahl limit when the surface density exceeds $4 \times 10^{14} \text{ g/cm}^3$. In contrast to General Relativity (GR), where compactness is unlikely to approach the black hole limit, our study reveals a different trend. We draw the relation between mass and radius associated with the boundary density we have determined, and this diagram is consistent with other observational discoveries.

Keywords: Krori-Barua ansatz; Modified gravity; Compact stars.

I. INTRODUCTION

Anisotropic pressure has been imposed in many models developed to derive realistic stellar models within the Einstein general relativity context, and in modified gravity as well. These models are motivated by the claim that pressure at the core of the compact star model could have an anisotropic structure where the density exceeds the nuclear density 10^{15} g/cm^3 . Herrera and Santos [1] have looked into how things can be different in different directions, called local anisotropy, and how it influences whether self-gravitating systems stay stable or collapse under gravity. Other researchers have also explored this topic in related studies; see for example, [2]. More and more people are getting interested in anisotropic fluids, which are fluids where the pressure pushing outwards isn't the same in all directions. Recent studies suggest that forcing these fluids to be the same in all directions, known as enforcing local isotropy, might not be the best approach. It could make it harder to accurately model objects influenced by their gravity. In compact objects like stars, many different things are happening that can cause pressure to be different in different directions. So, it's really important to figure out ways to accurately describe these situations where pressure isn't the same everywhere. Thus, investigating possible techniques for obtaining precise solutions that characterize anisotropic fluid distributions is crucial. Readers are referred to [3] for a thorough examination of the causes and effects of local anisotropy in astrophysical objects.

The configuration and characteristics of compact celestial entities pose a fundamental challenge within the realm of general relativity. This area of research was inaugurated as early as 1916 by Schwarzschild, who derived the inner solution for a spherical object with a uniform density, featuring zero pressure at its vacuum boundary [4]. Although theoretically simple and of limited relevance to real stellar objects, the Schwarzschild interior solution garnered significant attention, leading to intensive examination of its properties and extensions [5–10]. A pivotal

*Electronic address: nashed@bue.edu.eg

†Electronic address: bamba@sss.fukushima-u.ac.jp

milestone in the advancement of relativistic astrophysics can be attributed to the contributions of Tolman [11, 12] and Oppenheimer and Volkoff [13] (TOV), who derived the structural equations for compact, spherically symmetric general relativistic objects in a static configuration.

Both theoretical and numerical explorations of the TOV equation culminated in the determination of the maximum mass limit for neutron stars, which was identified to be approximately $3.2M_{\odot}$ [14]. This outcome was achieved through the application of causality principles, the highly rigid equation of state characterized by $p = \rho c^2$, and Le Chatelier's principle. Importantly, this result remains true when the equation of state (EoS) is not fully understood within a certain range of densities. Conversely, Chandrasekhar [15] derived a limiting mass of approximately $1.4M_{\odot}$ for white dwarfs. Both theoretical reasoning and observational findings subsequently gave rise to the widely accepted notion, upheld for a considerable duration, that the mass distribution of neutron stars is concentrated around a value roughly in the vicinity of $1.4M_{\odot}$ [16]. This mass value is a consequence of the understanding that neutron stars rely on the dominant pressure exerted by neutron degeneracy following the collapse of a white dwarf. For a neutron star with a mass of approximately $1.4M_{\odot}$, the associated radius is expected to be around $10 \approx 15\text{km}$, with average ρ to be roughly $6 \times 10^{14}\text{g/cm}^3$.

Nevertheless, the conventional perspective on the masses of neutron stars has undergone a significant transformation in recent times, as more precise determinations of neutron star masses have become increasingly accessible [17]. Extensive astronomical observations and the detection of gravitational waves have definitively shown that the masses of neutron stars span a significantly wider range than what one would expect solely based on the Chandrasekhar limit. In their study, Margalit and Metzger [18] combined electromagnetic (EM) and gravitational wave (GW) data from the binary neutron star (NS) merger GW170817 to constrain the radii and maximum mass M_{max} of neutron stars. They established an upper limit of $M_{max} = 2.17M_{\odot}$ (90% confidence), which is arguably less model-dependent than other current constraints. This limitation is more stringent and less reliant on specific models compared to alternative constraints. The study conducted by Shibata et al. [19] based on the same event indicated that the equation of state for neutron matter must exhibit significant rigidity, suggesting that M_{max} of neutron stars should considerably exceed $2M_{\odot}$. This mass threshold is essential to allow for the formation of a stable, long-lasting massive neutron star as the outcome of the merger in binary systems like GW170817, where the initial combined mass overrides $2.73M_{\odot}$. Furthermore, considering the absence of a relativistic optical counterpart, we can deduce M_{max} value for the neutron star in the range of approximately $2.15 - 2.25M_{\odot}$. Comparable estimates for the neutron star's maximum mass have been derived in the studies conducted by Ruiz and Rezzolla [20, 21], respectively. Using the Shapiro delay, alternative methods for estimating the masses of neutron stars produced results of approximately $1.928 \pm 0.017M_{\odot}$ for the pulsar PSR J1614-2230 1, and a mass of $2.14^{+0.10}_{-0.09}M_{\odot}$ for the Millisecond Pulsar MSP J0740+6620 [22].

One significant pathway for potentially elucidating the elevated mass values of neutron stars involves the realm of modified gravity. Modified theories have primarily appeared to account for contemporary expansion of the cosmos. To delve into in-depth conversations concerning the accelerating Universe, the concept of dark energy, and matters pertaining to modified gravity, consider consulting the reviews listed in the provided references [23–26].

Modified theories of gravity can potentially provide fresh perspectives on comprehending the composition of compact celestial bodies. Several essential characteristics of star structures, including maximum masses, moments of inertia, and mass-radius relationships, differ from standard general relativity within modified gravitational theories [27]. These alterations stem from the modification of the Poisson equation for gravitational potential, resulting in changes to the radius, central density, mass, and luminosity of the stars [27]. The measured masses of many neutron stars, which fall in the range of approximately $2M_{\odot}$, have led to disagreements with predictions from realistic equations of state for dense matter. As a result, certain softer equations, especially those incorporating hyperons, have been ruled out [27]. Advanced gravity theories that extend beyond general relativity have the potential to mitigate or resolve these discrepancies by introducing corrections into the generalized hydrostatic equilibrium equations of extended stellar models [27].

Different forms of general relativity modifications have been put forth to explain the observed properties of compact celestial bodies, such as neutron stars, and their mass distribution. These extensions encompass various gravity theories, including $f(\mathcal{G})$, $f(\mathcal{R}, \mathcal{G})$, $f(\mathcal{R}, T)$, and $f(\mathcal{R}, L_m)$ types. For a concise overview of the astrophysical consequences of the aforementioned theories, refer to ([27] and references therein).

A captivating subset of modified gravity models, commonly denoted as $f(\mathcal{R}, \mathcal{G})$ [25, 28, 29], arises from the inspiration of string theory and is known as modified Gauss-Bonnet gravity. It provides an interesting way to efficiently generate the late-time acceleration phase. Gravitation theories that combine the Gauss-Bonnet and Ricci scalars are found in the literature; studies of this type of theory can be found in [30, 31]. The modified Gauss-Bonnet theory holds a significant role in the field of astrophysics due to its potential to reshape our understanding of the universe and its fundamental structures. This theory, inspired by string theory and emerging from the broader landscape of modified gravity, offers a novel perspective on gravity's behavior in extreme astrophysical environments. It opens the door to exploring phenomena that cannot be explained by conventional general relativity such as the nature of compact objects like neutron stars and black holes, their mass distributions, and the equations of state for dense matter. More-

over, the modified Gauss-Bonnet theory provides a framework to investigate the late-time acceleration of the universe, a critical aspect of modern cosmology. Its flexibility in accommodating various forms of gravitational interactions and its ability to address long-standing astrophysical anomalies make it an essential tool for astrophysicists seeking to comprehend the cosmos in its entirety. This theory's potential to reconcile theory with observations and offer new avenues for astrophysical exploration makes it a prominent and vital component of contemporary astrophysical research. The goal of this study is to leverage the higher-order aspects of Gauss-Bonnet gravity, drawn from its known properties and advantages. Gauss-Bonnet gravity finds frequent use in theoretical physics to extend general relativity by accommodating higher-order curvature corrections. This extension can provide insights into various phenomena such as black hole physics, cosmology, and gravitational wave physics, thereby offering a more comprehensive understanding of gravity beyond standard Einsteinian theory. Hence, the implicit motivation for employing Gauss-Bonnet gravity could be to investigate its implications within the astrophysical framework, determining its potential to yield a consistent stellar model. This aspect will be explored throughout the study.

The study's structure includes a review in Section II for the framework $\mathcal{R} + f(\mathcal{G})$ modified theory. Section III applies quadratic $\mathcal{R} + f(\mathcal{G}) = \mathcal{R} + \alpha_1 \mathcal{G}^2$ gravity to the KB stellar model, ensuring compatibility with the Schwarzschild exterior vacuum solution through imposed matching conditions. In Section IV, We use astrophysical data to study radius and mass of the pulsar $\mathcal{J}0740 + 6620$ to limit the dimensionless α_1 . Additionally, we assess the model's validity by applying diverse stability criteria. In Section V, we derive the Equations of State (EoS) governing the matter sector. We also analyze the associated mass-radius diagram and present the study's conclusion in Section VI.

II. DISTRIBUTION OF ANISOTROPIC MATTER IN $\mathcal{R} + f(\mathcal{G})$ GRAVITY

The overarching action for the modified $f(\mathcal{G})$ is as follows [32],

$$\mathcal{L} = \frac{1}{2\kappa^2} \int d^4x \sqrt{-g} [\mathcal{R} + f(\mathcal{G})] + \int d^4x \sqrt{-g} \mathcal{L}_M. \quad (1)$$

In this context, $f(\mathcal{G})$ represents the arbitrary Gauss-Bonnet (GB) function with \mathcal{G} being the GB, while κ^2 stands for the coupling constant. The GB expression, \mathcal{G} , is defined as follows:

$$\mathcal{G} = \mathcal{R}^2 - 4\mathcal{R}_{\zeta\eta}\mathcal{R}^{\zeta\eta} + \mathcal{R}_{\zeta\eta\mu\nu}\mathcal{R}^{\zeta\eta\mu\nu}. \quad (2)$$

In this context, $\mathcal{R}_{\zeta\eta}$ and $\mathcal{R}_{\zeta\eta\mu\nu}$ represent the Ricci and Reimann tensors, respectively. When we vary Eq. (1) concerning $g_{\zeta\eta}$, it yields the following set of fourth-order non-linear field equations:

$$\begin{aligned} G_{\zeta\eta} - [2\mathcal{R}g_{\zeta\eta}\nabla^2 + 2\mathcal{R}\nabla_{\zeta}\nabla_{\eta} + 4g_{\zeta\eta}\mathcal{R}^{\mu\nu}\nabla_{\mu}\nabla_{\nu} + 4\mathcal{R}_{\zeta\eta}\nabla^2 - 4\mathcal{R}_{\zeta}^{\mu}\nabla_{\eta}\nabla_{\mu} - 4\mathcal{R}_{\eta}^{\mu}\nabla_{\zeta}\nabla_{\mu} - 4\mathcal{R}_{\zeta\mu\eta\nu}\nabla^{\mu}\nabla^{\nu}]f_{\mathcal{G}} \\ - \frac{1}{2}g_{\zeta\eta}f + [2\mathcal{R}\mathcal{R}_{\zeta\eta} - 4\mathcal{R}_{\zeta}^{\mu}\mathcal{R}_{\mu\eta} - 4\mathcal{R}_{\zeta\mu\eta\nu}R^{\mu\nu} + 2\mathcal{R}_{\zeta}^{\mu\nu\delta}\mathcal{R}_{\eta\mu\nu\delta}]f_{\mathcal{G}} = \kappa^2 T_{\zeta\eta}, \end{aligned} \quad (3)$$

In this context, we have the d'Alembertian operator denoted as $\square = \nabla^2 = \nabla_{\zeta}\nabla^{\zeta}$, the Einstein tensor $G_{\zeta\eta} = \mathcal{R}_{\zeta\eta} - \frac{1}{2}g_{\zeta\eta}\mathcal{R}$, the function f represented as $f \equiv f(\mathcal{G})$, and $f_{\mathcal{G}}$ denoting the partial derivative of $f(\mathcal{G})$ concerning \mathcal{G} . The Einstein equations can be restored simply by setting $f(\mathcal{G}) = 0$. Here $T_{\zeta\eta}$ is the energy-momentum tensor defined as:

$$T_{\zeta\eta} = -\frac{2}{\sqrt{-g}} \frac{\delta(\sqrt{-g}\mathcal{L}_M)}{\delta g^{\zeta\eta}}. \quad (4)$$

Furthermore, the energy-momentum tensor that depends on the metric can take the following shape:

$$T_{\zeta\eta} = g_{\zeta\eta}\mathcal{L}_M - 2\frac{\partial\mathcal{L}_M}{\partial g^{\zeta\eta}}. \quad (5)$$

The anisotropic for of $T_{\zeta\eta}$ is defined as:

$$T^{\zeta}_{\eta} = (\rho + p_t)V^{\zeta}V_{\eta} - p_t\delta^{\zeta}_{\eta} + (p_r - p_t)\xi^{\zeta}\xi_{\eta}. \quad (6)$$

The energy-momentum tensor, T^{μ}_{ν} , is defined as:

$$T^{\mu}_{\nu} = \text{diag}(-\rho c^2, p_r, p_t, p_t).$$

The trace part of Eq.(3) is given by

$$-\mathcal{R} + 2\mathcal{G}f_{\mathcal{G}}(\mathcal{G}) + 2\mathcal{R}\nabla^2 f_{\mathcal{G}}(\mathcal{G}) - 4R_{\alpha\beta}\nabla^\alpha\nabla^\beta f_{\mathcal{G}}(\mathcal{G}) = \kappa^2 T.$$

It is significant to mention that in $f(\mathcal{G})$, the standard conservation equation of the stress-energy tensor is not satisfied, i.e., covariant derivative of $T_{\alpha\beta}$ is non-zero ($\nabla^\alpha T_{\alpha\beta} \neq 0$). This fact can be justified by taking the covariant derivative of Eq.(3), which on combing with the Bianchi identity $\nabla^\alpha G_{\alpha\beta}$, gives

$$\kappa^2\nabla^\alpha T_{\alpha\beta} = -\frac{1}{2}g_{\alpha\beta}\nabla^\alpha f(\mathcal{G}). \quad (7)$$

It can be easily seen from the above expression that in general, the conservation law does not hold for this gravitational theory. For the linearized $\mathcal{R} + f(\mathcal{G})$ gravity, the corresponding field equations, as the linear results, are the same as those of the linearized R gravity. In this limit, the gravitational coupling constant κ^2 does not differ from Einstein's $8\pi G/c^4$ [33].

III. THE ANISOTROPIC GAUSS-BONNET COUPLED WITH MATTER MODEL

In this section, we will seek an anisotropic solution within the framework of $R + f(\mathcal{G})$. To achieve this, we will employ the following particular model,

$$f(\mathcal{G}) = \alpha_1 \mathcal{G}^2, \quad (8)$$

where α_1 is a dimensional quantity that has the unit $length^6$. In this investigation, we will introduce the following line element:

$$ds^2 = g_{\mu\nu}dx^\mu dx^\nu = -e^\psi c^2 dt^2 + e^\lambda dr^2 + r^2(d\theta^2 + \sin^2\theta d\phi^2). \quad (9)$$

The metric functions, represented as ψ and λ , are two functions that depend solely on the radial coordinate r . Consequently, we can calculate $\sqrt{-g} = r^2 \sin\theta e^{(\psi+\lambda)/2}$, as well as the four-velocity vector. $v^\mu = (ce^{-\psi/2}, 0, 0, 0)$.

By using Eq. (9) for computation, we obtain the Ricci and Gauss-Bonnet scalars as follows:

$$\begin{aligned} \mathcal{R} &= \frac{(\lambda'r^2 - 4r)\psi' - 2\psi''r^2 - \psi'^2r^2 + 4\lambda'r + 4e^\lambda - 4}{2r^2e^\lambda}, \\ \mathcal{G} &= \frac{2e^{-2\lambda}\{[\lambda'(e^\lambda - 3) - (e^\lambda - 1)\psi']\psi' - (2e^\lambda - 2)\psi''\}}{r^2}, \end{aligned} \quad (10)$$

where $' \equiv d/dr$ and $'' \equiv d^2/dr^2$, and so on. Utilizing the Ricci and Gauss-Bonnet values provided by Eq. (10) in the field equations (3) after applying the constraints (8), we obtain:

$$\begin{aligned} \rho &= \frac{1}{c^2\kappa^2r^6e^{4\lambda}} \left(32\alpha_1r^2(e^\lambda - 1)^2\psi'''' + 32r\alpha_1(r(e^\lambda - 1)\psi' + (7r - 3re^\lambda)\psi'_1 - 4e^\lambda + 4)(e^\lambda - 1)\psi'''' - 16\alpha_1\psi'r^2(e^\lambda - 1) \right. \\ &\times (e^\lambda - 3)\lambda''' + 24\alpha_1r^2(e^\lambda - 1)^2a''^2 - 8\left(8r^2\left(e^\lambda - \frac{5}{2}\right)(e^\lambda - 1)\lambda'' + r^2(e^\lambda - 1)^2a'^2 + 9\left(\left(e^\lambda - \frac{19}{9}\right)ra'_1 \right. \right. \\ &+ \left. \frac{16}{9}e^\lambda - \frac{16}{9}\right)r(e^\lambda - 1)\psi' - 11\left(\left(e^\lambda\right)^2 - \frac{64}{11}e^\lambda + \frac{61}{11}\right)r^2\lambda'^2 - 28\left(e^\lambda - \frac{17}{7}\right)r(e^\lambda - 1)a'_1 - 24(e^\lambda - 1)^2\alpha_1\psi'' \\ &- 16\left(r(e^\lambda - 1)(e^\lambda - 2)a' - 7/2r\left(\frac{45}{7} + (e^\lambda)^2 - \frac{48}{7}e^\lambda\right)\lambda' - 12 + 16e^\lambda - 4(e^\lambda)^2\right)\psi'r\alpha_1\lambda'' - 2\alpha_1r^2(e^\lambda - 1)^2a'^4 \\ &+ 4\alpha_1\lambda'r^2(e^\lambda - 1)(e^\lambda - 3)\psi'^3 + 22\alpha_1\left(r^2\left((e^\lambda)^2 - \frac{54}{11}e^\lambda + \frac{47}{11}\right)\lambda'^2 + \frac{40}{11}r(e^\lambda - 1)\left(e^\lambda - \frac{11}{5}\right)a'_1 + \frac{48}{11}(e^\lambda - 1)^2\right)\psi'^2 \\ &\left. + 24\psi'\alpha_1\left(\left(e^{2\lambda} - \frac{35}{3}e^\lambda + 14\right)r^2\lambda'^2 + \frac{10}{3}\left(\frac{33}{5} - \frac{34}{5}e^\lambda + e^{2\lambda}\right)ra'_1 - 16e^\lambda + 4e^{2\lambda} + 12\right)\psi' + r^4e^{3\lambda}(e^\lambda - 1 + a'_1r)\right), \end{aligned} \quad (11)$$

$$\begin{aligned} p_r &= \frac{1}{\kappa^2(e^\lambda)^4r^5} \left\{ 8\alpha_1r(e^\lambda - 1)^2a''^2 - 16r\alpha_1\psi'(e^\lambda - 1)(e^\lambda - 3)\psi'''' - 8\psi'(r(e^\lambda - 1)(e^\lambda - 5)a' - 2(e^\lambda - 3) \right. \\ &(r(e^\lambda - 3)\lambda' + 2e^\lambda - 2))\alpha_1\psi'' + 8r\alpha_1a'^2(e^\lambda - 3)^2a''_1 + 2\alpha_1r(e^\lambda - 1)^2a'^4 + 4(e^\lambda - 3)(r(e^\lambda - 3)\lambda' + 4e^\lambda - 4)\alpha_1\psi^3 \\ &\left. - 6(e^\lambda - 3)\left(r(e^\lambda - 7)\lambda' + \frac{8}{3}e^\lambda - 8\right)\lambda'\alpha_1\psi'^2 + r^4\psi'(e^\lambda)^3 - r^3(e^\lambda)^3(e^\lambda - 1)\right\}, \end{aligned} \quad (12)$$

$$\begin{aligned}
p_t = & \frac{1}{4\kappa^2 (e^\lambda)^4 r^5} \left(64\alpha_1 r^2 \psi' (e^\lambda - 1) \psi'''' + 96r\alpha_1 \left(\frac{2}{3}r (e^\lambda - 1) \psi'' + \psi' \left(r (e^\lambda - 1) \psi' - \frac{8}{3} \left(e^\lambda - \frac{7}{4} \right) r a'_1 + \frac{8}{3} - \frac{8}{3} e^\lambda \right) \right) \psi'''' \right. \\
& - 32 \alpha_1 r^2 \psi'^2 (e^\lambda - 3) \lambda''' + 32r\alpha_1 \left(4r (e^\lambda - 1) a' - (3e^\lambda - 7) r \lambda' + 5 - 6e^\lambda + (e^\lambda)^2 \right) \psi''^2 + \left(160 \left(\frac{13}{5} - e^\lambda \right) \psi' r^2 \alpha_1 \lambda'' \right. \\
& + 32 \alpha_1 r^2 (e^\lambda - 1) \psi'^3 - 304 \left(\left(-\frac{33}{19} + e^\lambda \right) r \lambda' - \frac{2}{19} (e^\lambda - 1) (e^\lambda - 13) \right) r \alpha_1 \psi'^2 + 304 \alpha_1 \left(\left(e^\lambda - \frac{73}{19} \right) r^2 \lambda'^2 \right. \\
& - 2/19 r \left((e^\lambda)^2 - 24 e^\lambda + 43 \right) \lambda' - \frac{24}{19} + \frac{24}{19} e^\lambda \left. \right) \psi' + 2r^5 (e^\lambda)^3 \left. \right) \psi'' - 48 \psi'^2 r \left((e^\lambda - 7/3) r \psi' - 3r (e^\lambda - 5) \lambda' - \frac{8}{3} e^\lambda \right. \\
& + 8) \alpha_1 \psi_1'' - 16 \left(r (e^\lambda - 2) \lambda' - \frac{5}{2} + 3e^\lambda - 1/2 (e^\lambda)^2 \right) r \alpha_1 \psi'^4 + 96 \left(r^2 \left(e^\lambda - \frac{10}{3} \right) \lambda'^2 - \frac{1}{6} r \left(-20 e^\lambda + 31 + (e^\lambda)^2 \right) \lambda' \right. \\
& + 2e^\lambda - 2) \alpha_1 \psi'^3 + \left(-80 \left(e^\lambda - \frac{42}{5} \right) r^2 \alpha_1 (\lambda')^3 + 8 \alpha_1 r \left(141 + (e^\lambda)^2 - 34 e^\lambda \right) \lambda'^2 - 192 (e^\lambda - 3) \alpha_1 \lambda' \right. \\
& \left. + r^5 (e^\lambda)^3 \right) \psi'^2 - r^4 (e^\lambda)^3 (-2 + \lambda' r) a' - 2r^4 \lambda' (e^\lambda)^3 \left. \right). \tag{13}
\end{aligned}$$

It's evident that t density and the components of the pressures are altered and become identical with the GR solution when considering $\alpha_1 = 0$ (as discussed in [34] and [35]).

A. Krori-Barua model

Because Eqs. (11), (12), and (13) form complex systems comprising three non-linear differential equations with five unknowns, namely, ψ , λ , ρ , p_r , and p_t additional conditions are required to render these systems solvable. There are various approaches to impose these two constraints, with one option being to adopt specific equations of state (EoS). However, this method may not be particularly advantageous since the aforementioned systems, namely, Eqs. (11), (12), and (13), involve fourth-order differential equations. The most effective approach we can employ is to prescribe specific forms for the ansatz of ψ and λ . In this study, we will utilize the KB metric potentials, as presented in [36]. Anisotropic compact star models in the Krori-Barua spacetime in GR have been studied in Refs. [37–42] and in modified theories of gravity in Refs. [43–53].

$$\psi(r) = n_0 (r/R_s)^2 + n_1, \quad \lambda(r) = n_2 (r/R_s)^2, \tag{14}$$

with R_s representing the radius surface of the pulsar, and n_0, n_1, n_2 are parameters that will be fixed from through the junction conditions. For the sake of unit adjustment, we assume:

$$\alpha_1 = \alpha_2 R_s^6. \tag{15}$$

Using Eqs. (14), (15), in Eqs. (11), (12) and (13), we obtain the explicate forms of energy-density, and the components of pressure as:

$$\begin{aligned}
\rho &= \frac{1}{\kappa^2 e^{\frac{4n_2 r^2}{R_s^2}} R_s^2 r^6 c^2} \left(4480 \alpha_2 n_2^3 n_0 e^{\frac{n_2 r^2}{R_s^2}} r^6 - 384 \alpha_2 n_2^3 n_0 e^{\frac{2n_2 r^2}{R_s^2}} r^6 - 1728 \alpha_2 n_0^2 n_2^2 e^{\frac{n_2 r^2}{R_s^2}} r^6 + 352 \alpha_2 n_0^2 n_2^2 e^{\frac{2n_2 r^2}{R_s^2}} r^6 \right. \\
&+ 64 \alpha_2 n_0^3 n_2 e^{\frac{2n_2 r^2}{R_s^2}} r^6 - 256 \alpha_2 n_0^3 n_2 e^{\frac{n_2 r^2}{R_s^2}} r^6 + 64 \alpha_2 R_s^4 n_0^2 e^{\frac{n_2 r^2}{R_s^2}} r^2 - 32 \alpha_2 R_s^4 n_0^2 e^{\frac{2n_2 r^2}{R_s^2}} r^2 - 64 \alpha_2 n_0^3 e^{\frac{2n_2 r^2}{R_s^2}} R_s^2 r^4 \\
&+ 128 \alpha_2 n_0^3 e^{\frac{n_2 r^2}{R_s^2}} R_s^2 r^4 + 2560 \alpha_2 n_2^2 n_0 R_s^2 r^4 - 64 \alpha_2 n_0^2 n_2 R_s^2 r^4 + 1152 \alpha_2 R_s^4 n_0 n_2 r^2 - e^{\frac{3n_2 r^2}{R_s^2}} R_s^2 r^4 + e^{\frac{4n_2 r^2}{R_s^2}} R_s^2 r^4 \\
&- 5376 \alpha_2 n_2^3 n_0 r^6 + 1504 \alpha_2 n_0^2 n_2^2 r^6 + 192 \alpha_2 n_0^3 n_2 r^6 - 32 \alpha_2 R_s^4 n_0^2 r^2 - 64 \alpha_2 n_0^3 R_s^2 r^4 - 768 \alpha_2 R_s^6 n_0 e^{\frac{n_2 r^2}{R_s^2}} \\
&+ 384 \alpha_2 R_s^6 n_0 e^{\frac{2n_2 r^2}{R_s^2}} + 64 \alpha_2 n_0^4 e^{\frac{n_2 r^2}{R_s^2}} r^6 - 32 \alpha_2 n_0^4 e^{\frac{2n_2 r^2}{R_s^2}} r^6 + 384 \alpha_2 R_s^6 n_0 + 2 n_2 e^{\frac{3n_2 r^2}{R_s^2}} r^6 - 32 \alpha_2 n_0^4 r^6 \\
&+ 128 \alpha_2 n_0^2 n_2 e^{\frac{n_2 r^2}{R_s^2}} R_s^2 r^4 - 64 \alpha_2 n_0^2 n_2 e^{\frac{2n_2 r^2}{R_s^2}} R_s^2 r^4 - 1664 \alpha_2 R_s^4 n_0 n_2 e^{\frac{n_2 r^2}{R_s^2}} r^2 + 512 \alpha_2 R_s^4 n_0 n_2 e^{\frac{2n_2 r^2}{R_s^2}} r^2 \\
&\left. + 512 \alpha_2 n_2^2 n_0 e^{\frac{2n_2 r^2}{R_s^2}} R_s^2 r^4 - 2816 \alpha_2 n_2^2 n_0 e^{\frac{n_2 r^2}{R_s^2}} R_s^2 r^4 \right), \\
p_r &= \frac{1}{\kappa^2 e^{\frac{4n_2 r^2}{R^2}} R^2 r^4} \left(2 n_0 e^{\frac{3n_2 r^2}{R^2}} r^4 - 384 \alpha_2 n_0^2 n_2 e^{\frac{n_2 r^2}{R^2}} R^2 r^2 + 576 \alpha_2 n_0^2 n_2 R^2 r^2 + 64 \alpha_2 n_0^2 n_2 e^{\frac{2n_2 r^2}{R^2}} R^2 r^2 \right. \\
&+ 960 \alpha_2 n_0^2 n_2^2 e^{\frac{n_2 r^2}{R^2}} r^4 - 2016 \alpha_2 n_0^2 n_2^2 r^4 + 576 \alpha_2 n_0^3 n_2 r^4 - 96 \alpha_2 n_0^2 n_2^2 e^{\frac{2n_2 r^2}{R^2}} r^4 + 64 \alpha_2 n_0^3 n_2 e^{\frac{2n_2 r^2}{R^2}} r^4 \\
&- 384 \alpha_2 n_0^3 n_2 e^{\frac{n_2 r^2}{R^2}} r^4 - 576 \alpha_2 R^4 n_0^2 e^{\frac{n_2 r^2}{R^2}} + 416 \alpha_2 R^4 n_0^2 - 64 \alpha_2 n_0^4 e^{\frac{n_2 r^2}{R^2}} r^4 + 32 \alpha_2 n_0^4 r^4 + 160 \alpha_2 R^4 n_0^2 e^{\frac{2n_2 r^2}{R^2}} \\
&\left. + 32 \alpha_2 n_0^4 e^{\frac{2n_2 r^2}{R^2}} r^4 + 64 \alpha_2 n_0^3 e^{\frac{2n_2 r^2}{R^2}} R^2 r^2 + 64 \alpha_2 n_0^3 R^2 r^2 - 128 \alpha_2 n_0^3 e^{\frac{n_2 r^2}{R^2}} R^2 r^2 + e^{\frac{3n_2 r^2}{R^2}} R^2 r^2 - e^{\frac{4n_2 r^2}{R^2}} R^2 r^2 \right), \\
p_t &= \frac{1}{\kappa^2 e^{\frac{4n_2 r^2}{R^2}} R^4 r^4} \left(-n_2 e^{\frac{3n_2 r^2}{R^2}} R^2 r^4 - r^6 n_0 n_2 e^{\frac{3n_2 r^2}{R^2}} + r^6 n_0^2 e^{\frac{3n_2 r^2}{R^2}} + 2 n_0 e^{\frac{3n_2 r^2}{R^2}} R^2 r^4 + 192 \alpha_2 R^6 n_0^2 e^{\frac{n_2 r^2}{R^2}} \right. \\
&+ 32 \alpha_2 R^6 n_0^2 e^{\frac{2n_2 r^2}{R^2}} - 2560 r^6 \alpha_2 n_0^3 n_2^2 + 5376 r^6 \alpha_2 n_0^2 n_2^3 + 256 r^6 \alpha_2 n_0^4 n_2 + 32 \alpha_2 n_0^4 R^2 r^4 + 192 \alpha_2 n_0^3 R^4 r^2 \\
&- 224 \alpha_2 R^6 n_0^2 + 896 \alpha_2 n_0^2 n_2 e^{\frac{n_2 r^2}{R^2}} R^4 r^2 - 64 \alpha_2 n_0^2 n_2 e^{\frac{2n_2 r^2}{R^2}} R^4 r^2 + 704 \alpha_2 n_0^2 n_2^2 e^{\frac{n_2 r^2}{R^2}} R^2 r^4 + 32 \alpha_2 n_0^2 n_2^2 e^{\frac{2n_2 r^2}{R^2}} R^2 r^4 \\
&- 64 \alpha_2 n_0^3 n_2 e^{\frac{2n_2 r^2}{R^2}} R^2 r^4 - 128 \alpha_2 n_0^3 n_2 e^{\frac{n_2 r^2}{R^2}} R^2 r^4 - 640 r^6 \alpha_2 n_0^2 n_2^3 e^{\frac{n_2 r^2}{R^2}} + 768 r^6 \alpha_2 n_0^3 n_2^2 e^{\frac{n_2 r^2}{R^2}} \\
&- 128 r^6 \alpha_2 n_0^4 n_2 e^{\frac{n_2 r^2}{R^2}} - 64 \alpha_2 n_0^4 e^{\frac{n_2 r^2}{R^2}} R^2 r^4 + 32 \alpha_2 n_0^4 e^{\frac{2n_2 r^2}{R^2}} R^2 r^4 + 64 \alpha_2 n_0^3 e^{\frac{2n_2 r^2}{R^2}} R^4 r^2 - 256 \alpha_2 n_0^3 e^{\frac{n_2 r^2}{R^2}} R^4 r^2 \\
&\left. - 1088 \alpha_2 n_0^2 n_2 R^4 r^2 - 3040 \alpha_2 n_0^2 n_2^2 R^2 r^4 + 576 \alpha_2 n_0^3 n_2 R^2 r^4 \right). \tag{16}
\end{aligned}$$

Furthermore, we present the force with anisotropic, $F_a = \frac{2\Delta}{r}$, which arises from the pressure difference. In situations with significant anisotropy $0 < r \leq R_s$, where $\Delta > 0$, it necessitates that $p_t > p_r$ throughout the star's interior. Conversely, in the mild anisotropy case, where $\Delta < 0$, it requires that $p_r > p_t$ within the pulsar.

B. Junction conditions

To address the equation of motions under specified junction conditions at $r = R_s$, where $p_r = 0$, the inner metric described by Eq. (9) necessitates the application of these matching conditions. This can be achieved by smoothly

connecting the interior metric at $r = R_s$ to Schwarzschild's exterior metric, which is expressed as:¹

$$ds^2 = - \left(1 - \frac{2GM}{c^2 r} \right) c^2 dt^2 + \frac{dr^2}{\left(1 - \frac{2GM}{c^2 r} \right)} + r^2 (d\theta^2 + \sin^2 \theta d\phi^2), \quad (19)$$

where, as seen from a point at an infinite distance, M denotes the star's gravitational mass. We apply the junction conditions as follows:

$$\psi(r = R_s) = \ln(1 - C), \quad \lambda(r = R_s) = -\ln(1 - C), \quad \text{and} \quad p_r(r = R_s) = 0, \quad (20)$$

with C being figured as:

$$C = \frac{2GM}{c^2 R_s}, \quad (21)$$

With the radial pressure from Eq. (16) and the KB ansatz (14), the parameters $\{n_0, n_1, n_2\}$ can be expressed with respect to $\alpha_2 C$ s.

IV. CONSTRAINTS ON ASTROPHYSICS AND STABILITY DERIVED FROM PULSAR $\mathcal{J}0740 + 6620$ OBSERVATIONS

Now, we specifically employ restrictions on M and R from the pulsar $\mathcal{J}0740 + 6620$ to calculate the quadratic gravity correction parameter's value α_2 . Additionally, to calculate the quadratic gravity correction parameter's value. As previously stated in the introduction, it is crucial to emphasize that precise observational data plays an immensely significant role in restricting α_2 . Initially, we need to address our selection of $\mathcal{PSRJ}0740 + 6620$ to constrain the form of $f(\mathcal{G})$ theory under consideration.

A. Constraints on mass and radius derived from $\mathcal{J}0740 + 6620$

Next, we employ the values of M and R of $\mathcal{PSRJ}0740 + 6620$, as $M = 2.07 \pm 0.11 M_\odot$ and $R_s = 12.34_{-1.67}^{+1.89}$ km, as documented in [54]. These measurements combine data from NICER and XMM to limit α_2 . The mass function is defined as follows:

$$m(r) = 4\pi \int_0^r \rho(\zeta) \zeta^2 d\zeta. \quad (22)$$

Returning to the density profile described in Eq. (16), in the context of the model $R + f(\mathcal{G}) = R + \alpha_1 \mathcal{G}^2$, we generate the plots shown in Fig. 1 for various numerical value of the parameter α_2 .

- In the case of $\alpha_2 = 0$, which corresponds to the GR scenario, the constant's numerical values are set as follows: $\{n_0 \approx 0.491, n_1 = -1.1756, n_2 = 0.684\}$.
- With $\alpha_2 = 0.0004$, we find $1.96 M_\odot$ with $R_s \approx 12.65$ km, and $C \approx 0.47$. This leads to: $\{\alpha_2 = 0.0004, C = 0.47, n_0 = 0.493, n_1 = -1.177, n_2 = 0.684\}$.

¹ To justify the use of Schwarzschild solution as an exterior solution for our system we will apply the form of Schwarzschild spacetime to the field equations of $f(\mathcal{G}) = \alpha_1 \mathcal{G}^2$. For this purpose, we get the following non-vanishing components:

$$\begin{aligned} tt - \text{component} &\equiv \frac{1152\alpha_1 M^3 G^3 (67GM - 32Rc^2)}{c^8 R^6}, & rr - \text{component} &\equiv \frac{1152\alpha_1 M^3 G^3 (11GM - 4Rc^2)}{c^8 R^6}, \\ \theta\theta - \text{component} &\equiv \frac{1152\alpha_1 M^3 G^3 (41GM - 18Rc^2)}{c^8 R^6}. \end{aligned} \quad (17)$$

If we calculate the above quantities numerically using the data of the pulsar under consideration which are $M = 2.07 \pm 0.11 M_\odot$ and $R_s = 12.34_{-1.67}^{+1.89}$ km and $\alpha_1 = 0.0004$ the following numerical values are obtained:

$$tt - \text{component} \equiv 7.089001308 \times 10^{-10}, \quad rr - \text{component} \equiv 5.866809379 \times 10^{-11}, \quad \theta\theta - \text{component} 3.609693140 \times 10^{-10} \quad (18)$$

while the Schwarzschild mass term has an order ~ 0.5 .

The above numerical values indicate that we can use the Schwarzschild solution as an exterior solution for the theory under consideration.

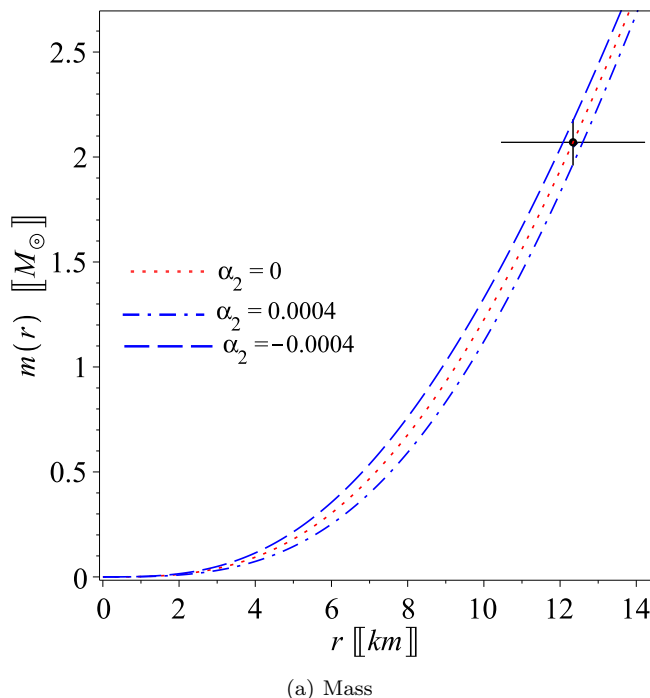


Figure 1: Mass given by Eq. (22) for pulsar $\mathcal{J}0740 + 6620$ is shown to represent the limitations of observation on its radius and mass ($R_s = 12.35 \pm 0.11$ km, $M = 2.07 \pm 0.11 M_\odot$) as per [54]. For $\alpha_2 = -0.0004$, we employ model parameters of approximately [$C \approx 0.524$, $n_0 \approx 0.489$, $n_1 \approx -1.174$, $n_2 = 0.684$]. For $\alpha_2 = 0.0004$, we utilize [$C = 0.47$, $n_0 = 0.493$, $n_1 = -1.177$, $n_2 = 0.684$]. For $\alpha_2 = 0$ GR, we use [$n_0 \approx 0.491$, $n_1 = -1.1756$, $n_2 = 0.684$].

- When $\alpha_2 = -0.0004$, the gravitational mass is approximately $2.22 M_\odot$ with $R_s \approx 11.96$ km, and $C \approx 0.524$. These values determine the numerical constants as follows: $\{\alpha_2 = -0.0004, C \approx 0.524, n_0 \approx 0.489, n_1 \approx -1.174, n_2 = 0.684\}$.

B. Geometric component

We must highlight that the metric components g_{tt} and g_{rr} should not display any singularities within the star's interior. The ansatz given by Eq. (14) guarantees regularity of these potentials at the central region because $g_{tt}(r=0) = e^\psi \neq 0$ and $g_{rr}(r=0) = 1$. Meanwhile, the way these potentials behave inside the star at any given radial position is shown in Fig. 2 (a).

Additionally, we express the redshift function on the KB potentials in relation to the quadratic form of $\mathcal{R} + f(\mathcal{G})$ gravity.

$$Z(r) = \frac{1}{\sqrt{-g_{tt}}} - 1 = \frac{1}{\sqrt{e^{n_0(r/R_s)^2 + n_1}}} - 1. \quad (23)$$

We have generated Z plot for $\mathcal{J}0740 + 6620$, varying α_2 as depicted in plot 2(b). When $\alpha_1 = 0$ (which corresponding to GR), $Z(r \rightarrow 0)$ yields $Z(0) \approx 0.806$, while $Z(r \rightarrow R_s)$ is $Z_s = Z_{R_s} \approx 0.4$. When considering $\alpha_2 = -0.0004$, Z reaches its maximum value at the core with $Z(0) \approx 0.832$, which is greater from GR. It then gradually reduces as we approach the surface, with $Z_s \approx 0.405$, a value close to that of GR which is below 2 as indicated in [55–58]. Likewise, for $\alpha_2 = 0.0004$, we observe the maxima of $Z(r \rightarrow 0)$ is $Z(0) \approx 0.774$, which is lower than the corresponding GR value. This maximum redshift then gradually diminishes as we approach the surface, with the redshift at the surface measuring approximately $Z_s \approx 0.4072$ a value close to the GR prediction.

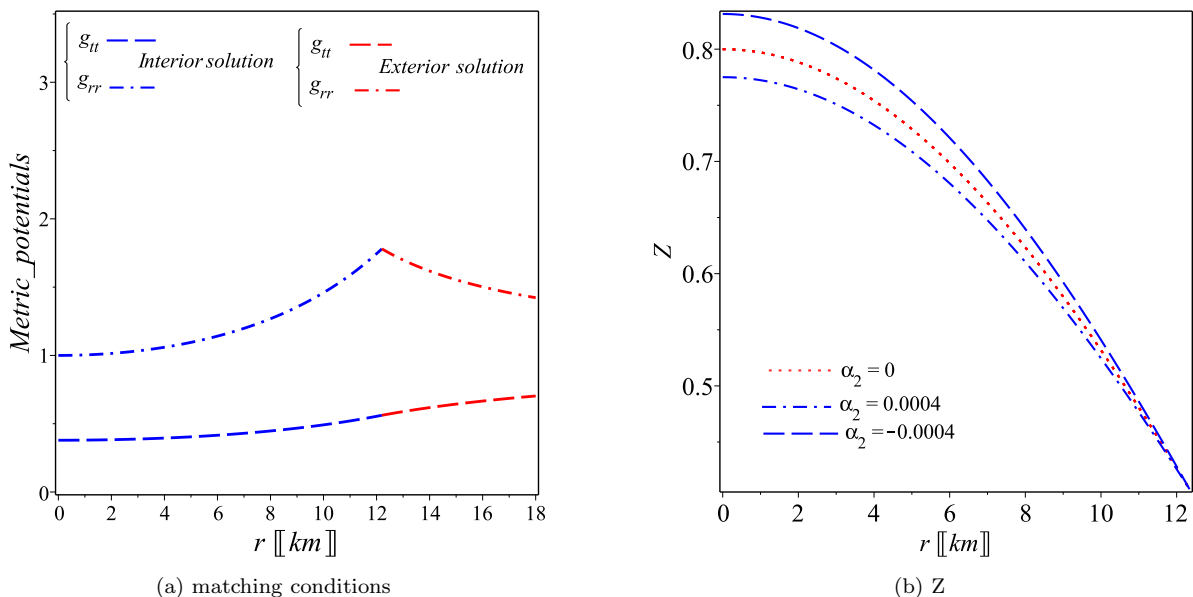


Figure 2: The geometric aspect of pulsar $\mathcal{J}0740 + 6620$, as depicted in (a), illustrates g_{tt} and g_{rr} using the KB, and the vacuum is the Schwarzschild exterior solution. These graphical representations serve to confirm the metric potentials' finite values throughout the interior of the pulsar and their seamless connection; (b) the redshift function (23), when considering values of α_2 equal to 0, as well as approximately ± 0.0004 , exhibits a peak redshift at the central point ≈ 0.8 , which then consistently reduces to approximately 0.4 as $r \rightarrow R_s$, across all scenarios.

C. Matter sector

By referring to Equ. (16) in conjunction with the numerical values in Subsection IV A, we can generate visual representations of ρ , p_r and p_t as functions of the radial coordinate, as shown in the Fig. 3(a)–(c). Clearly, ρ , p_r and p_t adhere to the stability criteria. Furthermore, we graphically represent $\Delta(r)$, in Fig. 3(d). It's important to highlight that in situations of substantial anisotropy, such as in our current investigation, an additional positive force, proportional to Δ/r , becomes a significant factor. This opposing force counteracts gravity, allowing the star to support high mass and achieve enhanced compactness which we will provide in details in Subsection IV G.

It's important to provide numerical values for certain physical parameters of pulsar $\mathcal{J}0740 + 6620$, as projected by the current model. These values are as follows: With $\alpha_2 = 0.0004$, the core density amounts to approximately $\rho_{\text{core}} \approx 6.68 \times 10^{14} \text{ g/cm}^3$, which is approximately $2.5(\rho_{\text{nuc}})$, and $p_{r \rightarrow 0}$, is roughly $7.81 \times 10^{33} \text{ dyn/cm}^2$, approximately equal to the core tangential pressure, $p_{t(\text{core})}$. At the pulsar's surface, the density is approximately $\rho_s \approx 4.14 \times 10^{14} \text{ g/cm}^3$, which is approximately $1.5(\rho_{\text{nuc}})$. The radial pressure at the surface, $p_{r(R_s)}$, is approximately 0 dyn/cm^2 , and the tangential pressure at the surface, $p_{t(R_s)}$, is approximately $4.01 \times 10^{33} \text{ dyn/cm}^2$.

For $\alpha_2 = -0.0004$, the central density amounts to approximately $\rho_{\text{core}} \approx 7.78 \times 10^{14} \text{ g/cm}^3$, which is approximately $2.9(\rho_{\text{nuc}})$. The pressure $p_{r \rightarrow 0}$, is approximately $1.104 \times 10^{34} \text{ dyn/cm}^2$, approximately equal to the core tangential pressure, $p_{t(\text{core})}$. At the pulsar's surface, we observe the density to be approximately $\rho_s \approx 4.1 \times 10^{14} \text{ g/cm}^3$, which is roughly 1.4 times the nuclear density (ρ_{nuc}). The radial pressure at the surface, $p_{r(R_s)}$, is nearly 0 dyn/cm^2 , while the tangential pressure at the surface, $p_{t(R_s)}$, is approximately $3.9 \times 10^{33} \text{ dyn/cm}^2$.

As explained in Section III, we have employed the KB ansatz (14) to close the system (11)–(13) instead of relying on EoS's. Consequently, we define $\eta := r/R_s$ and express asymptotically Eqs. (16) to order $O(\eta^2)$. These equations yield the following relationships:

$$p_r(\rho) \approx c_1\rho + c_2, \quad p_t(\rho) \approx c_3\rho + c_4, \quad (24)$$

where c_1 , c_2 , c_3 , and c_4 , are entirely dictated by specific parameters in the model space, which are defined in Appendix A. Notably, we can represent the previously mentioned equations in a way that is more intuitively understandable from a physical perspective.

$$p_r(\rho) \approx v_r^2(\rho - \rho_1), \quad p_t(\rho) \approx v_t^2(\rho - \rho_2), \quad (25)$$

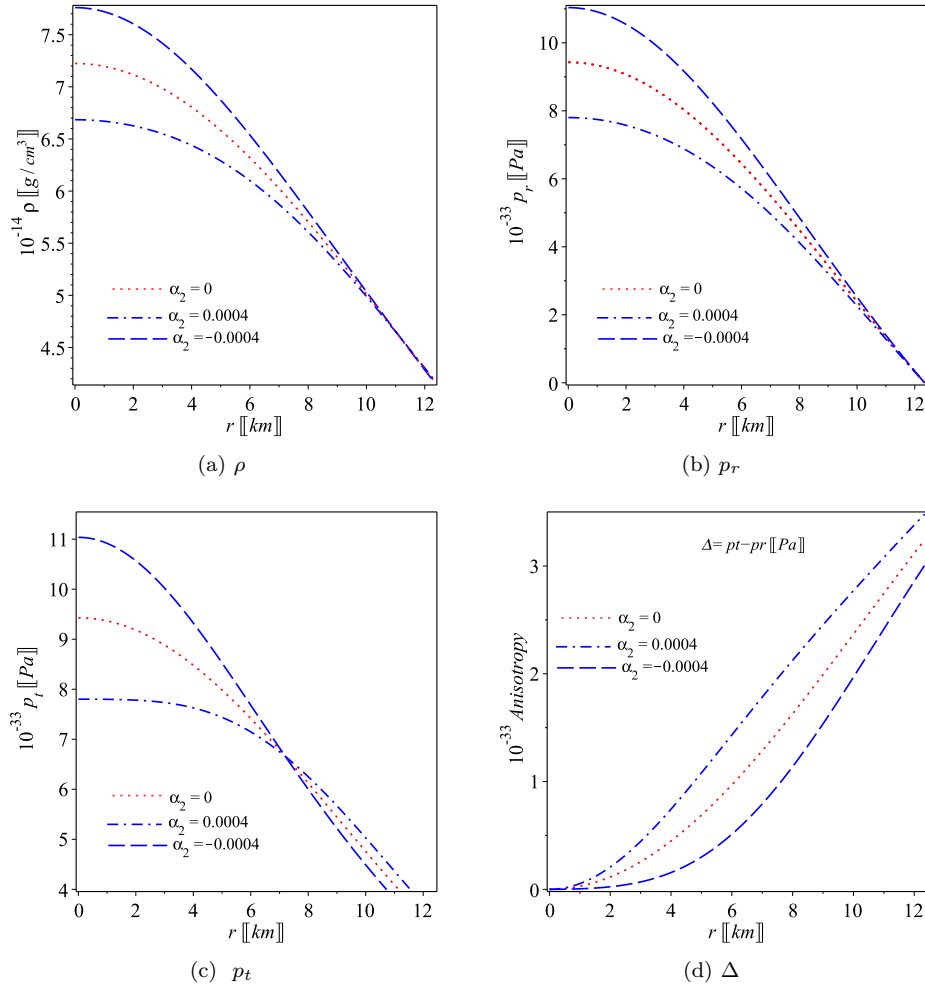


Figure 3: Characteristics of pulsar under consideration, as depicted in (a) to (c), illustrate ρ , p_r and p_t of Eq. (16). These visual representations are provided for three scenarios: $\alpha_2 = 0, \pm 0.0004$. The illustrations confirm that ρ and the components of the pressures maintain limited values through the inner of the pulsar and consistently reduce as we approach the surface (d) depicts the anisotropy using the three cases: $\alpha_2 = 0, \pm 0.0004$. It's evident that at the central point, the anisotropy vanishes, indicated by $p_t = p_r$. However, in regions away from the center, Δ takes on positive values (reflecting strong anisotropy with $p_t > p_r$), which, in turn, gives rise to a repulsive force denoted as $F_a = 2\Delta/r$. This force plays a pivotal role in adjusting the pulsar's radius.

In this case, the quantities assume a more comprehensible form: $v_t^2 = c_1$, $v_r^2 = c_3$ are the speeds of sound in the tangential and radial directions moreover, c_2/c_1 is the density defined as $-\rho_1$ and so on. It's worth noting that ρ_1 corresponds ρ_s and verifies $p_r(\rho_s) = 0$. This doesn't hold true to ρ_2 because p_t may not necessarily be zero at the surface.

D. Zeldovich's criterion

A crucial requirement to ensure the stability of a star, as discussed in [59], is that $p_r(r \rightarrow 0)$ should not $\rho(r \rightarrow 0)$, i.e.

$$\frac{p_r(0)}{c^2 \rho(0)} \leq 1. \quad (26)$$

Referring to Eq. (16), we can derive $\rho(r \rightarrow 0)$ and $p_r(r \rightarrow 0)$.

$$\begin{aligned} \rho_{r \rightarrow 0} &= 3 \frac{n_2 (1 + 32\alpha_2 n_0^2 n_2 - 3226 \alpha_2 n_2^2 n_0)}{c^2 R_s^2 \kappa^2}, \\ p_{r \rightarrow 0} &= \frac{2 n_0 - 1376 \alpha_2 n_0^2 n_2^2 + (256 \alpha_2 n_0^3 - 1) n_2}{\chi^2 R^2}. \end{aligned} \quad (27)$$

Employing the previously obtained numerical values for the pulsar $\mathcal{J}0740 + 6620$ in Subsection IV A, when $\alpha_2 = 0.0004$, the Zeldovich inequality (26) translates to $\frac{p_r(0)}{c^2 \rho(0)} = 0.102$, which is less than 1. Similarly, for $\alpha_2 = -0.0004$, the inequality leads to $\frac{p_r(0)}{c^2 \rho(0)} = 0.105$, which is also less than 1. This affirms that the Zeldovich criterion is satisfied in both scenarios. One of the most exciting issues is the sign of the matter trace inside neutron stars. Usually, the trace is assumed to be negative for normal matter (electromagnetic field and non-interacting particles). However, this condition could be broken in strongly interacting systems as mentioned by Zeldovich. This case within the theory under consideration, $\mathcal{R} + f(\mathcal{G})$ gravity, is not satisfied, i.e., the trace of the solution presented in this study has a positive value which is in agreement with what presented in [60].

E. Conditions related to energy distributions

It is advantageous to express the Eq. (3) as:

$$G_{\mu\nu} = \kappa (\mathfrak{T}_{\mu\nu} + \mathfrak{T}_{\mu\nu}^{geom}) = \kappa T_{\mu\nu}^{eff}. \quad (28)$$

Here, $G_{\mu\nu} := \mathcal{R}_{\mu\nu} - g_{\mu\nu} \mathcal{R}/2$ represents the Einstein tensor, which accounts for the corrections introduced by the quadratic form in $f(\mathcal{G})$ theory [61]

$$\begin{aligned} \mathfrak{T}_{\mu\nu}^{geom} &= -\frac{1}{\kappa^2} \left([2\mathcal{R}g_{\zeta\eta}\nabla^2 + 2\mathcal{R}\nabla_\zeta\nabla_\eta + 4g_{\zeta\eta}\mathcal{R}^{\mu\nu}\nabla_\mu\nabla_\nu + 4\mathcal{R}_{\zeta\eta}\nabla^2 - 4\mathcal{R}_\zeta^\mu\nabla_\eta\nabla_\mu - 4\mathcal{R}_\eta^\mu\nabla_\zeta\nabla_\mu - 4\mathcal{R}_{\zeta\mu\eta\nu}\nabla^\mu\nabla^\nu]f_{\mathcal{G}} \right. \\ &\quad \left. - \frac{1}{2}g_{\zeta\eta}f + [2\mathcal{R}\mathcal{R}_{\zeta\eta} - 4\mathcal{R}_\zeta^\mu\mathcal{R}_{\mu\eta} - 4\mathcal{R}_{\zeta\mu\eta\nu}R^{\mu\nu} + 2\mathcal{R}_\zeta^{\mu\nu\delta}\mathcal{R}_{\eta\mu\nu\delta}]f_{\mathcal{G}} \right), \end{aligned} \quad (29)$$

and $T_{\mu\nu}^{eff}$ is given by $T_{\mu\nu}^{eff} = \text{diag}(-\tilde{\rho}_1 c^2, \tilde{p}_{1r}, \tilde{p}_{1t}, \tilde{p}_{1t})$. It's important to note that the Ricci tensor in modified gravity of $\mathcal{R} + f(\mathcal{G})$ can be expressed as follows $\mathcal{R}_{\mu\nu} = \kappa (T_{\mu\nu}^{eff} - \frac{1}{2}g_{\mu\nu}T_{\mu\nu}^{eff})$. This can be recognized from Eq. (28). In this context, we can modify the energy conditions to encompass $\mathcal{R} + f(\mathcal{G})$ as:

- $\tilde{\rho}_1 \geq 0$, $\tilde{\rho}_1 c^2 + \tilde{p}_{1r} > 0$ and $\tilde{\rho}_1 c^2 + \tilde{p}_{1t} > 0$, specifically, (WEC).
- $\tilde{\rho}_1 c^2 + \tilde{p}_{1r} \geq 0$ and $\tilde{\rho}_1 c^2 + \tilde{p}_{1t} \geq 0$, namely, (NEC).
- $\tilde{\rho}_1 c^2 + \tilde{p}_{1r} + 2\tilde{p}_{1t} \geq 0$, $\tilde{\rho}_1 c^2 + \tilde{p}_{1r} \geq 0$ and $\tilde{\rho}_1 c^2 + \tilde{p}_{1t} \geq 0$.
- $\tilde{\rho}_1 \geq 0$, $\tilde{\rho}_1 c^2 - \tilde{p}_{1r} \geq 0$ and $\tilde{\rho}_1 c^2 - \tilde{p}_{1t} \geq 0$.

In Fig. 4, we plot the above conditions with possible values of α_2 . These plots confirm that the current model for pulsar $\mathcal{J}0740 + 6620$ is satisfied.

F. Causality properties of the model

Reflecting on the derived EoS (25), p_r and p_t are represented as:

$$v_r^2 = \frac{dp_r}{d\rho} = \frac{p_r'}{\rho'}, \quad v_t^2 = \frac{dp_t}{d\rho} = \frac{p_t'}{\rho'}. \quad (30)$$

Using Eq. (16), we derive derivatives of ρ , p_r and p_t , which are presented in the Appendix B, as detailed in Eqs. (B1)–(B3). We illustrate the propagation of c_s in both tangential and radial directions within pulsar $\mathcal{J}0740 + 6620$, considering various values of the model parameter α_2 . These visual representations are provided in plots 5(a) and (b) which confirm that the values of v_r^2/c^2 and v_t^2/c^2 fall within the range of $0 \leq v_r^2/c^2 \leq 1$ and $0 \leq v_t^2/c^2 \leq 1$, thereby

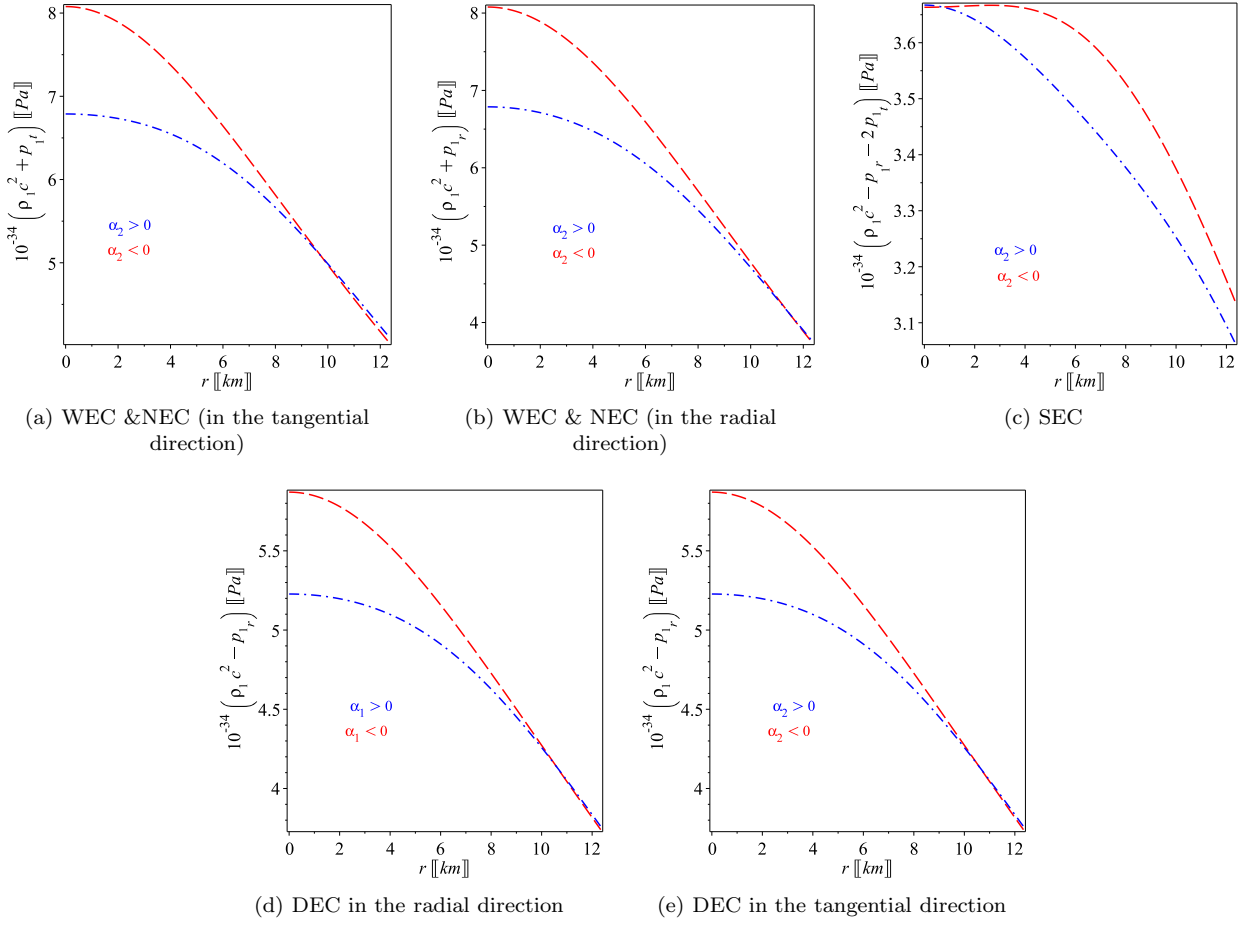


Figure 4: The graphical representations confirm the satisfaction of all the energy conditions of $T_{\mu\nu}^{eff}$, as elaborated in Subsection IV E. The scenarios where $\alpha_2 > 0$ and $\alpha_2 < 0$ correspond to the cases with $\alpha_2 = 0.0004$ and $\alpha_2 = -0.0004$ respectively.

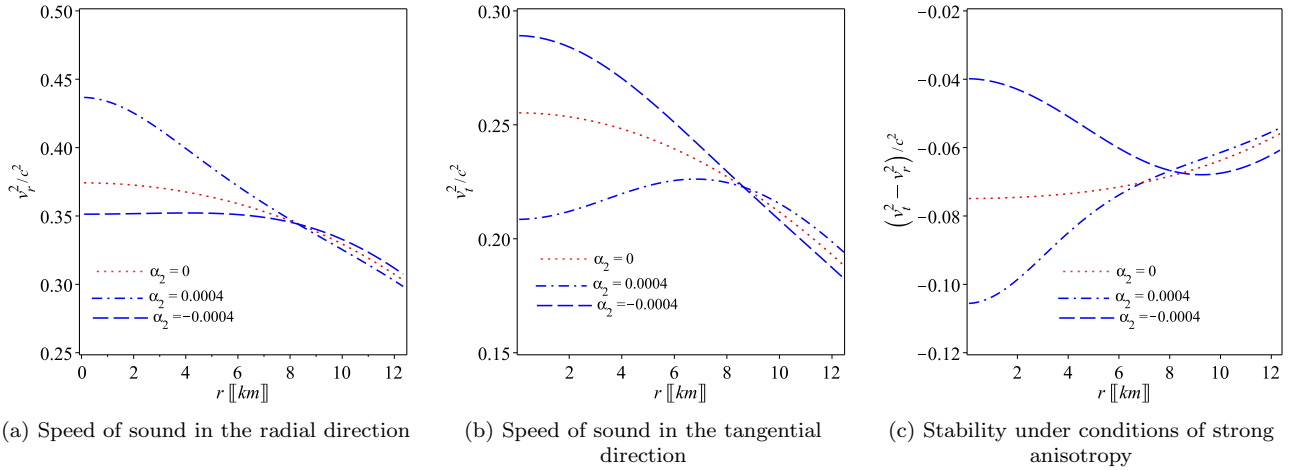


Figure 5: Sound speed of $\mathcal{J}0740 + 6620$ for $\alpha_2 = 0, \pm 0.0004$ is presented as follows: (a) and (b) illustrate the sound propagation as described by Eq. (30). In (c), the figures demonstrate that $(v_t^2 - v_r^2)/c^2 < 0$ required for a strongly anisotropic configuration.

satisfying the causality and stability conditions. As Fig. 5(c) shows the stability of an anisotropic stellar configuration is verified [62].

It's worth mentioning that the speed of sound both directions, (radial and tangential), undergoes changes as we move radially, as visualized in plots 5(a) and (b). When $\alpha_2 = 0.0004$, we observe that $0.30 < v_r^2/c^2 < 0.45$, and $0.19 < v_t^2/c^2 < 0.22$. In the case of $\alpha_2 = -0.0004$, we find that $0.33 < v_r^2/c^2 < 0.35$ and $0.19 < v_t^2/c^2 < 0.30$. The maximum bounds of these periods correspond to the speeds of sound as $r \rightarrow 0$.

G. Adiabatic indices and the state of hydrostatic equilibrium

In this section we are going to use another tool to test the stability of the model under consideration For this aim, we define the following quantities [63, 64]:

$$\gamma = \frac{4}{3} \left(1 + \frac{\Delta}{r|p'_r|} \right)_{max}, \quad \Gamma_r = \frac{\rho c^2 + p_r}{p_r} v_r^2, \quad \Gamma_t = \frac{\rho c^2 + p_t}{p_t} v_t^2, \quad (31)$$

where γ , define the adiabatic index and Γ_r and Γ_t are the adiabatic indices in the radial and tangential direction. Certainly, in the isotropic case where $\Delta = 0$, we have $\gamma = 4/3$. In the case of mild anisotropy where $\Delta < 0$, we find $\gamma < 4/3$, similar to what is observed in Newtonian theory. However, in the case of strong anisotropy, we have $\gamma > 4/3$. In neutral equilibrium $\Gamma = \gamma$, while $\Gamma \gamma$ to achieve a stable equilibrium [64, 65]. By leveraging Eqs. (16) we can determine (B2)–(B3), and show that $f(\mathcal{G})$ in its quadratic form offers a stable model for pulsar $\mathcal{J}0740 + 6620$, regardless of the specific values of α_2 , as shown in Fig. 6. As is clear from Fig. 6 (b) that the radial pressure diverges at the stellar surface because our model is self bound [66–68].

Next, we explore the hydrostatic equilibrium in the current model using the TOV equation. This equation has been modified to be applicable to a specific context of $\mathcal{R} + f(\mathcal{G})$ theory, and it takes the following form [11–13]:²

$$\mathcal{F}_a + \mathcal{F}_g + \mathcal{F}_h + \mathcal{F}_G = 0. \quad (32)$$

in this context, \mathcal{F}_h , \mathcal{F}_a , and \mathcal{F}_g , denote hydrostatic, anisotropic, and gravitational forces, along with the supplementary force \mathcal{F}_G arising from the effects of the quadratic $\mathcal{R} + f(\mathcal{G})$ gravity theory $f(\mathcal{G})$. Such forces are characterized as:

$$\begin{aligned} \mathcal{F}_a &= \frac{2\Delta}{r}, & \mathcal{F}_g &= -\frac{M_g}{r}(\rho c^2 + p_r)e^{\varrho/2}, \\ \mathcal{F}_h &= -p'_t, & \mathcal{F}_G &= -2\alpha_2(\mathcal{G}'). \end{aligned} \quad (33)$$

Within the force equation for \mathcal{F}_g , we present $\varrho := \psi - \lambda$, and M_g depicts, in three dimensions, the mass of an isolated system. This quantity is defined through the use of the expression presented in [69] adapted to the context of $\mathcal{R} + f(\mathcal{G})$ gravity

$$\begin{aligned} M_g(r) &= \int_V \left(\mathfrak{T}_1^r{}_r + \mathfrak{T}_1^\theta{}_\theta + \mathfrak{T}_1^\phi{}_\phi - \mathfrak{T}_1^t{}_t \right) \sqrt{-g} dV \\ &= e^{-\psi} (e^{\psi/2})' e^{\lambda/2} r = \frac{1}{2} r \psi' e^{-\varrho/2}. \end{aligned} \quad (34)$$

As a result, the gravitational force is expressed as $F_g = -\frac{20r}{R_s^2}(\rho c^2 + p_r)$. By employing Eqs. (16) and (B2)–(B3), we can verify Eq. (32) which ensure by plot 7.

V. THE RELATIONSHIP BETWEEN MASS AND RADIUS AND THE EQUATION OF STATE

Astrophysicists are still grappling with the enigmatic composition of matter within the cores of neutron stars, as these cores achieve densities greater than (ρ_{nuc}), an unexplored domain lying beyond the grasp of earthly laboratories. In spite that the EoS controlling the matter inside neutron stars is still unknown, measurements of their mass and radius in astrophysical settings may be able to constrain it. As a result, astrophysical observations can narrow down

² It is of interest to stress that the TOV equation given by Eq. (32) is different from the original one due to the extra term given by \mathcal{F}_G . The appearance of this term is due to the non-conservation given by Eq. (7).

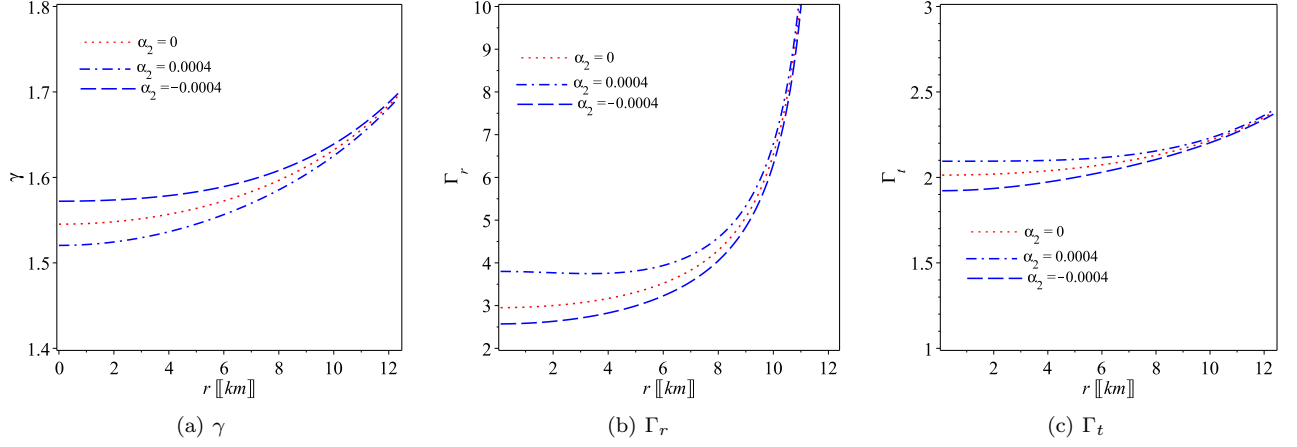


Figure 6: The adiabatic indices, as presented in Eq. (31), for $\mathcal{J}0740 + 6620$.

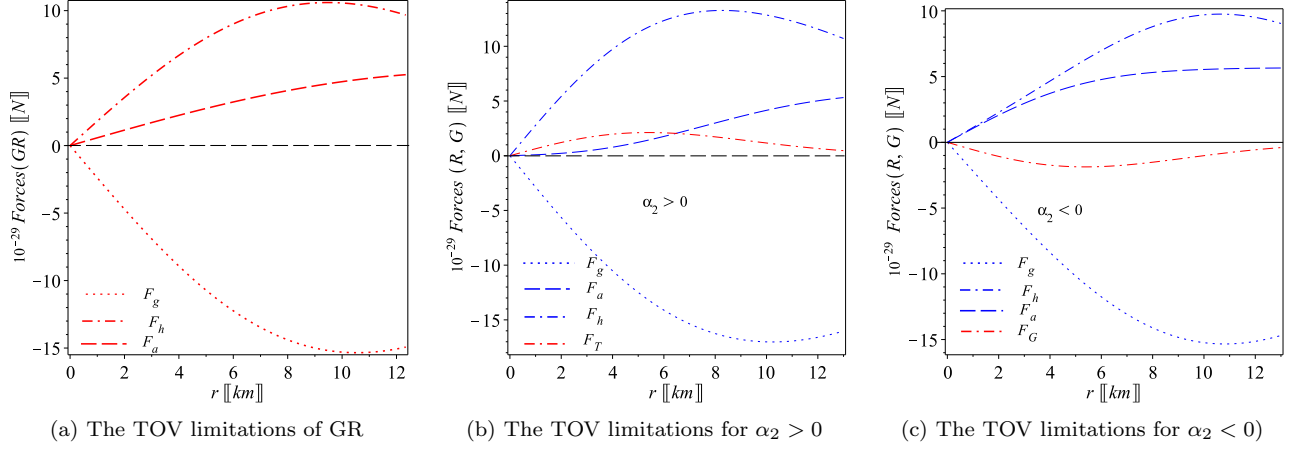


Figure 7: TOV constraint (32): Various forces, given by Eqs. (33), acting within the pulsar $\mathcal{J}0740 + 6620$ are depicted for $\alpha_2 = 0, \pm 0.0004$. In the case $\alpha_2 = 0.0004$ an extra negative force, further reinforcing the force of gravitational collapse. When $\alpha_2 = -0.0004$, introduces a positive additional force, that mitigates the collapsing force.

the mass-radius diagram linked to a particular EoS. Indeed, in this study, we do not enforce specific EoSs; instead, we employ the KB ansatz (14). However, EoS derived from this ansatz shows a relationship between ρ and pressure ((25)), which are mainly useful at the core because of their dependence on power series. Utilizing the numerical values provided in Section IV A for the pulsar $\mathcal{J}0740 + 6620$ and the equations of motion of $\mathcal{R} + f(\mathcal{G})$ given by Eqs. (16), we create Fig. 8.

In this study, concerning $\mathcal{J}0740 + 662$, we determine the BL as follows: For $\alpha_2 = \pm 0.0004$ we obtain $C \lesssim 0.86$ which results in slight modifications to the GR BL. This aligns with our observation that quadratic gravity in this scenario introduces an additional force to TOV equation. This opposing force counteracts gravity, allowing the pulsar to have greater mass and attain greater compactness. We assume a surface density of $\rho_s = 4 \times 10^{14} \text{ g/cm}^3$ for both $\alpha_2 = \pm 0.0004$. For various values of the compactness parameter in the range of $0 \leq C \leq 1$ we compute the density profile using Eq. (16) to derive the corresponding radius R . Likewise, we derive compactness-radius curves, as depicted in plot 9(a).

For the previously derived best-fit equations of state, MR curves are provided in plot 9(b) for positive and negative values of α_2 .

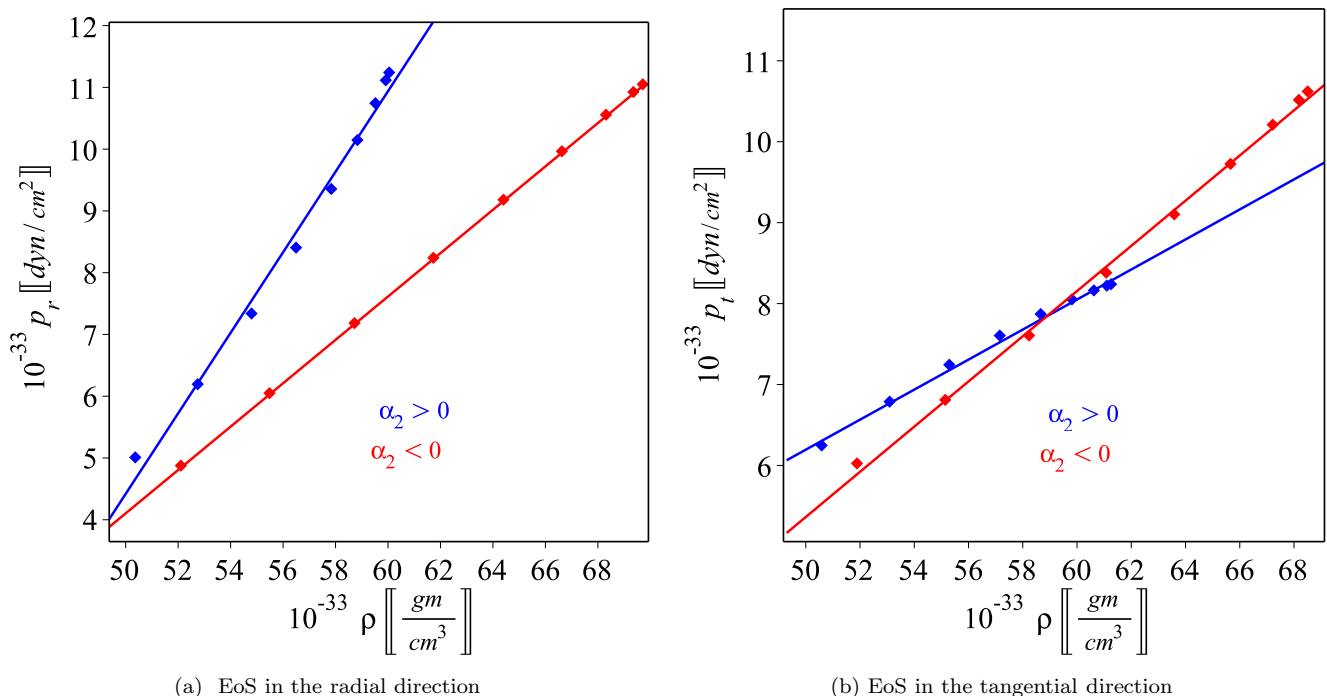


Figure 8: Optimal fit EoSs for the pulsar $\mathcal{J}0740 + 6620$, as shown in (a), involve the generation of a series of data for ρ and p_r using Eqs. (16) with $\alpha_2 = \pm 0.0004$. These observations are consistent with a linear EoS behavior ((b)). Likewise, when considering tangential EoS's when $\alpha_2 = \pm 0.0004$ The data points exhibit robust alignment with a linear trend and align with previously established results, particularly Eq. (25). This reaffirms the validity of these relationships within the pulsar's interior.

VI. CONCLUSION AND DISCUSSION

The Gauss-Bonnet term holds significant importance in the realms of differential geometry and theoretical physics. It plays a significant role in modern theoretical physics, particularly in the framework of gravitational theories in the frame of astrophysics and cosmology. The Gauss-Bonnet term is a topological invariant, and its quadratic form is often considered in higher-dimensional theories of gravity. In four spacetime dimensions, the Gauss-Bonnet term is a topological invariant and does not contribute to the equations of motion. However, in higher dimensions, it can significantly impact the dynamics of spacetime and matter fields.

Pulsars are crucial astronomical objects, serving as powerful tools for testing various physical theories, including general relativity and alternative theories of gravity. Understanding the behavior of pulsars in the presence of exotic terms in the Einstein-Hilbert action, such as the function $f(\mathcal{G})$ Gauss-Bonnet term, can shed light on the fundamental physics governing these astrophysical phenomena.

In this current study, we explored the quadratic $\mathcal{R} + f(\mathcal{G})$ gravity theory by subjecting it to scrutiny through the lens of astrophysical observations. We examined a plausible situation involving an anisotropic fluid, as is typical for the extremely dense material found within pulsars. Additionally, we supposed that the interior abide to the KB ansatz, which guarantees the smoothness of the inner geometry. Specifically, we leveraged precise measurements of M and R of $\mathcal{P}SRJ0740 + 6620$, which were determined as $M = 2.07 \pm 0.11M_\odot$ and a radius of $R_s = 12.34_{-1.67}^{+1.89}$ km, based on NICER+XMM observations [54]. These observations allowed us to delimit α_1 of $f(\mathcal{G})$ gravity, i.e. $[\alpha_1, C]$. Conversely, $\mathcal{P}SRJ0740 + 6620$ stands out as one of the most massive pulsars, rendering it an ideal candidate for assessing modified gravity theories.

We have shown the MR plot linked to the best-fit EoS, as shown in Fig. 9(b). When $\alpha_2 = 0.0004$ and with a surface density $\rho_s = 4 \times 10^{14}$ g/cm³ we obtained $M = 4.71M_\odot$ and $R_s = 12.6$ km. When $\alpha_2 = -0.0004$ and $\rho_s = 4.0 \times 10^{14}$ g/cm³, we obtained $M = 4.1M_\odot$ and $R_s = 14.4$ km. These values align perfectly with those observed in the pulsar $\mathcal{J}0740 + 6620$.

To summarize our results:

i- We have succeeded for the first time in constructing a stellar model within the framework of the quadratic form of $f(G)$.

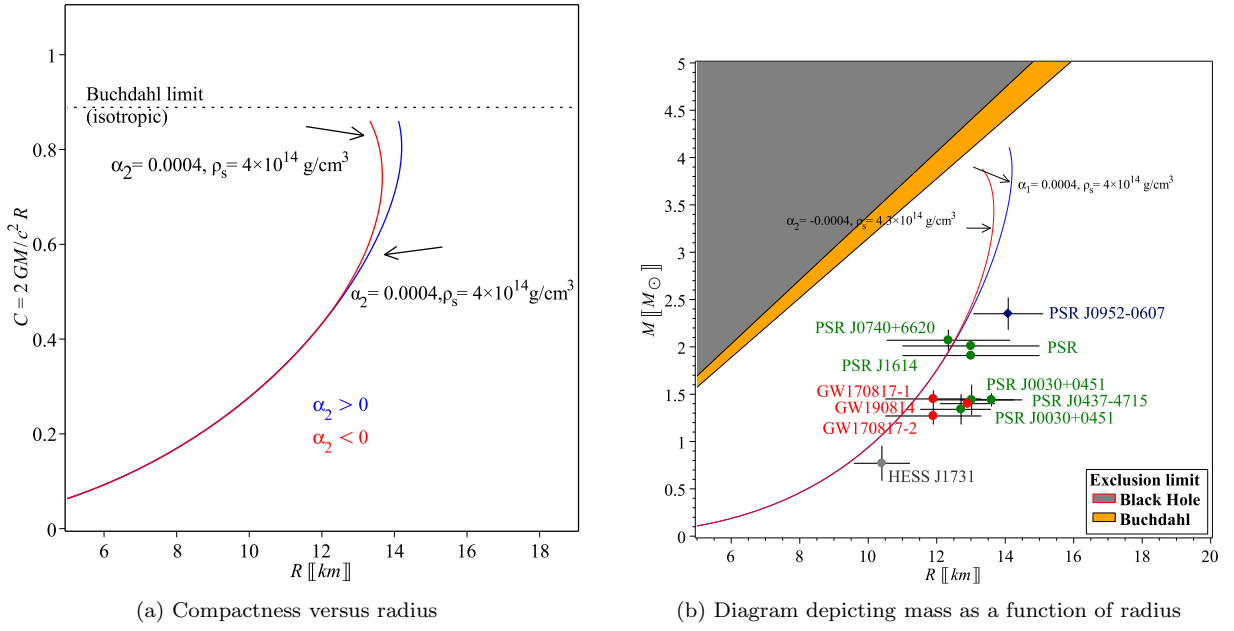


Figure 9: (a). Compactness versus radius plot: The dashed horizontal line denotes the BL at a compactness of $C = 8/9$. We illustrate the Compactness-radius curves associated with the optimal EoS fits as provided in Fig. 8. Furthermore, we depict Compactness-radius curves for $\rho_s = 4 \times 10^{14} \text{ g/cm}^3$. It's worth mentioning that for $\alpha_2 = 0.0004$ the compactness can be extended up to the BL of $C \rightarrow 8/9$ a characteristic shared with the GR model [35]. It is noteworthy that, intriguingly, when $\alpha_2 = 0.0004$ the extreme value of the compactness is below the BL for $\rho_s = 4 \times 10^{14} \text{ g/cm}^3$. The Mass-radius (MR) plot presented in (b), the colors gray (orange) area denotes the black hole limit. Likewise, in the case of positive/negative α_2 even at their maximum mass, the mass-radius curves do not cross the BL.

- ii- We have shown that our model is satisfactory from different requirements imposed on any physically admissible stellar model.
- iii- Finally, we derive the mass-radius diagram showing the capability of the obtained curves to match observational data of other pulsars.

Acknowledgments

The work of KB was partially supported by the JSPS KAKENHI Grant Number 21K03547 and 23KF0008.

A

Appendix A: The KB model and the induced EoSs

It has been shown that the KB ansatz relates the pressures and the density which effectively induces the EoSs as given by Eqs. (24). The coefficients in those equations are related to the model parameters as listed as below.

$$c_1 = \frac{1}{R_s^4 n_2^2} \left\{ 4 (256 \alpha_1 n_0^3 n_2 R_s^4 - 1376 \alpha_1 n_0^2 n_2^2 R_s^4 - n_2 R_s^4 + 2 n_0 R_s^4) n_2 + \left(\frac{7}{2} n_2^2 R_s^4 + 192 \alpha_1 n_0^3 n_2^2 R_s^4 - 6 n_0 n_2 R_s^4 - \frac{2464}{3} \alpha_1 n_0^2 n_2^3 R_s^4 \right) \right\} (54144 \alpha_1 n_0^2 n_2 - 501888 \alpha_1 n_2^2 n_0 + 90 + 6912 \alpha_1 n_0^3) c^2 (9024 \alpha_1 n_0^2 n_2 - 83648 \alpha_1 n_2^2 n_0 + 15 + 1152 \alpha_1 n_0^3)^{-2}, \quad (\text{A1})$$

$$c_2 = \frac{(256 \alpha_1 n_0^3 n_2 - 1376 \alpha_1 n_0^2 n_2^2 - n_2 + 2 n_0)}{\kappa R_s^2} + \frac{1}{R_s^2 n_2^2} \left\{ \frac{4 (256 \alpha_1 n_0^3 n_2 - 1376 \alpha_1 n_0^2 n_2^2 - n_2 + 2 n_0) n_2}{\kappa} + \frac{1}{\kappa} \left(\frac{7}{2} n_2^2 + 192 \alpha_1 n_0^3 n_2^2 - 6 n_0 n_2 - \frac{2464}{3} \alpha_1 n_0^2 n_2^3 \right) \right\} (54144 \alpha_1 n_0^2 n_2 - 501888 \alpha_1 n_2^2 n_0 + 90 + 6912 \alpha_1 n_0^3) (2496 \alpha_1 n_2^3 n_0 - 3 n_2 + 96 \alpha_1 n_0^2 n_2^2) (9024 \alpha_1 n_0^2 n_2 - 83648 \alpha_1 n_2^2 n_0 + 15 + 1152 \alpha_1 n_0^3)^{-2}, \quad (\text{A2})$$

$$c_3 = \frac{(18432 \alpha_1 n_0^3 R_s^2 c^2 - 6 R_s^2 c^2) n_2^2 - 68416 \alpha_1 n_0^2 R_s^2 c^2 n_2^3 + (18 n_0 \kappa R_s^2 c^2 - 768 \alpha_1 n_0^4 R_s^2 c^2) n_2 - 6 n_0^2 R_s^2 c^2}{R_s^2 (9024 \alpha_1 n_0^2 n_2 - 83648 \alpha_1 n_2^2 n_0 + 15 + 1152 \alpha_1 n_0^3) n_2^2}, \quad (\text{A3})$$

$$c_4 = \frac{1}{n_2 R_s^2 \kappa} \left\{ 68672 n_2^4 \alpha_1 n_0 - 55666688 n_2^5 \alpha_1^2 n_0^3 + 18743296 n_2^4 \alpha_1^2 n_0^4 + 53792 \alpha_1 n_0^2 n_2^3 - 2961408 n_2^3 \alpha_1^2 n_0^5 + 3 n_2^2 - 51264 \alpha_1 n_0^3 n_2^2 + 368640 n_2^2 \alpha_1^2 n_0^6 - 24 n_0 n_2 + 5184 n_2 \alpha_1 n_0^4 + 18 n_0^2 \right\} (9024 \alpha_1 n_0^2 n_2 - 83648 \alpha_1 n_2^2 n_0 + 15 + 1152 \alpha_1 n_0^3)^{-1}. \quad (\text{A4})$$

Using the above set of equations, one can find the physical quantities appear in Eq. (25) in terms of the model parameters, where $v_r^2 = c_1$, $\rho_1 = \rho_s = -c_2/c_1$, $v_t^2 = c_3$ and $\rho_2 = -c_4/c_3$.

Appendix B: Density and pressures gradients

Recalling the matter density and the pressures as obtained for the quadratic polynomial $f(R)$ gravity, namely Eqs. (16), we obtain the gradients of these quantities with respect to the radial distance as below

$$\rho' = \frac{-2 e^{-4 \frac{n_2 r^2}{R_s^2}}}{R_s^4 \kappa^2 r^7 c^2} \left(256 r^6 \alpha_2 n_0^2 n_2^2 R_s^2 + 256 r^6 \alpha_2 n_0^3 n_2 R_s^2 + 192 r^4 \alpha_2 n_0^2 n_2 R_s^4 - 3840 r^2 \alpha_2 R_s^6 n_0 n_2 - 10240 r^6 \alpha_2 n_2^3 n_0 R_s^2 - 7168 r^4 \alpha_2 n_2^2 n_0 R_s^4 - 192 r^8 \alpha_2 n_0^4 n_2 e^{\frac{n_2 r^2}{R_s^2}} - 13440 r^8 \alpha_2 n_2^4 n_0 e^{\frac{n_2 r^2}{R_s^2}} + 5184 r^8 \alpha_2 n_0^2 n_2^3 e^{\frac{n_2 r^2}{R_s^2}} + 768 r^8 \alpha_2 n_0^3 n_2^2 e^{\frac{n_2 r^2}{R_s^2}} - 128 r^2 \alpha_2 R_s^6 n_0^2 e^{\frac{n_2 r^2}{R_s^2}} - 128 r^4 \alpha_2 a_0^3 e^{\frac{n_2 r^2}{R_s^2}} R_s^4 + 64 r^8 \alpha_2 n_0^4 e^2 \frac{n_2 r^2}{R_s^2} n_2 + 768 r^8 \alpha_2 n_2^4 n_0 e^2 \frac{n_2 r^2}{R_s^2} - 704 r^8 \alpha_2 n_0^2 n_2^3 e^2 \frac{n_2 r^2}{R_s^2} - 128 r^8 \alpha_2 n_0^3 n_2^2 e^2 \frac{n_2 r^2}{R_s^2} + 64 r^2 \alpha_2 R_s^6 n_0^2 e^2 \frac{n_2 r^2}{R_s^2} + 64 r^4 \alpha_2 n_0^3 e^2 \frac{n_2 r^2}{R_s^2} R_s^4 + r^6 e^3 \frac{n_2 r^2}{R_s^2} n_2 R_s^2 + r^4 e^3 \frac{n_2 r^2}{R_s^2} R_s^4 - r^4 e^4 \frac{n_2 r^2}{R_s^2} R_s^4 - 1152 R_s^8 \alpha_2 n_0 e^2 \frac{n_2 r^2}{R_s^2} + 64 r^4 \alpha_2 n_0^3 R_s^4 + 64 r^2 \alpha_2 R_s^6 n_0^2 + 21504 n_2^4 r^8 \alpha_2 n_0 - 6016 n_2^3 r^8 \alpha_2 n_0^2 - 768 n_2^2 r^8 \alpha_2 n_0^3 + 128 n_2 r^8 \alpha_2 n_0^4 + 2304 R_s^8 \alpha_2 n_0 e^{\frac{n_2 r^2}{R_s^2}} - 2 r^8 n_2^2 e^3 \frac{n_2 r^2}{R_s^2} - 1152 R_s^8 \alpha_2 n_0 + 5632 r^2 \alpha_2 R_s^6 n_0 n_2 e^{\frac{n_2 r^2}{R_s^2}} + 7808 r^4 \alpha_2 R_s^4 n_0 n_2^2 e^{\frac{n_2 r^2}{R_s^2}} - 320 r^4 \alpha_2 n_0^2 n_2 e^{\frac{n_2 r^2}{R_s^2}} R_s^4 - 384 r^6 \alpha_2 n_0^3 n_2 e^{\frac{n_2 r^2}{R_s^2}} R_s^2 - 384 r^6 \alpha_2 n_0^2 n_2^2 e^{\frac{n_2 r^2}{R_s^2}} R_s^2 + 8448 r^6 \alpha_2 n_2^3 n_0 e^{\frac{n_2 r^2}{R_s^2}} R_s^2 - 1792 r^2 \alpha_2 R_s^6 n_0 e^2 \frac{n_2 r^2}{R_s^2} n_2 - 1536 r^4 \alpha_2 R_s^4 n_0 n_2^2 e^2 \frac{n_2 r^2}{R_s^2} + 128 r^4 \alpha_2 n_0^2 n_2 e^2 \frac{n_2 r^2}{R_s^2} R_s^4 + 128 r^6 \alpha_2 n_0^3 n_2 e^2 \frac{n_2 r^2}{R_s^2} R_s^2 + 128 r^6 \alpha_2 n_0^2 n_2^2 e^2 \frac{n_2 r^2}{R_s^2} R_s^2 - 1024 r^6 \alpha_2 n_2^3 n_0 e^2 \frac{n_2 r^2}{R_s^2} R_s^2 \right), \quad (\text{B1})$$

$$\begin{aligned}
p'_r = & \frac{1}{R_s^4 \kappa^2 e^{\frac{4n_2 r^2}{R_s^2}} r^5} \left(2 \left(e^{\frac{n_2 r^2}{R_s^2}} \right)^4 R_s^4 r^2 + (-2 R_s^4 r^2 - 2 n_2 R_s^2 r^4 - 4 r^6 n_0 n_2) \left(e^{\frac{n_2 r^2}{R_s^2}} \right)^3 - 640 \alpha_2 \left(\frac{1}{5} n_2 (n_0 + 3 n_2) \right. \right. \\
& (n_0 - n_2) r^6 + 2/5 R_s^2 n_2 (n_2 + n_0) r^4 + 1/5 R_s^4 (6 n_2 + n_0) r^2 + R_s^6) n_0^2 \left(e^{\frac{n_2 r^2}{R_s^2}} \right)^2 + 2304 \alpha_2 n_0^2 \left(\frac{1}{6} n_2 (6 n_0 n_2 - 15 n_2^2 \right. \\
& + n_0^2) r^6 + 1/3 R_s^2 n_2 (n_0 + 3 n_2) r^4 + 1/9 R_s^4 \left(n_0 + \frac{33}{2} n_2 \right) r^2 + R_s^6) e^{\frac{n_2 r^2}{R_s^2}} - 1664 \left(\frac{2}{13} n_2 (n_0 + 21 n_2) (n_0 - 3 n_2) r^6 \right. \\
& \left. \left. + \frac{4}{13} R_s^2 n_2 (9 n_2 + n_0) r^4 + 1/13 R_s^4 (n_0 + 35 n_2) r^2 + R_s^6 \right) \alpha_2 n_0^2 \right), \tag{B2}
\end{aligned}$$

$$\begin{aligned}
p'_t = & \frac{1}{\kappa^2 e^{\frac{4n_2 r^2}{R_s^2}} R_s^6 r^5} \left\{ 2 r^6 ((-n_2 r^2 + R_s^2) n_0^2 + (n_2^2 r^2 - 3 n_2 R_s^2) n_0 + n_2^2 R_s^2) \left(e^{\frac{n_2 r^2}{R_s^2}} \right)^3 - 128 R_s^2 n_0^2 \alpha_2 (n_0 r^2 + R_s^2 \right. \\
& - n_2 r^2) (R_s^4 + r^2 R_s^2 n_2 + n_2 r^4 n_0 - n_2^2 r^4) \left(e^{\frac{n_2 r^2}{R_s^2}} \right)^2 - 768 \alpha_2 n_0^2 ((-1/6 n_2 r^6 R_s^2 - n_2^2 r^8) n_0^2 + (6 n_2^3 r^8 - 3 n_2^2 r^6 R_s^2 \\
& - 2 n_2 r^4 R_s^4 - \frac{2}{3} r^2 R_s^6) n_0 + \frac{43}{6} n_2^3 r^6 R_s^2 + \frac{23}{6} n_2 r^2 R_s^6 + 7 n_2^2 r^4 R_s^4 - 5 n_2^4 r^8 + R_s^8) e^{\frac{n_2 r^2}{R_s^2}} + 896 \alpha_2 n_0^2 \left(\frac{2}{7} n_2 r^6 (R_s^2 \right. \\
& - 8 n_2 r^2) n_0^2 - \frac{3}{7} r^2 \left(4 n_2 R_s^4 r^2 + R_s^6 - \frac{160}{3} r^6 n_2^3 + \frac{76}{3} n_2^2 R_s^2 r^4 \right) n_0 + R_s^8 - 48 n_2^4 r^8 + \frac{68}{7} n_2^2 r^4 R_s^4 + \frac{31}{7} n_2 r^2 R_s^6 \\
& \left. \left. + \frac{274}{7} n_2^3 r^6 R_s^2 \right) \right\}. \tag{B3}
\end{aligned}$$

-
- [1] L. Herrera and N. O. Santos, Phys. Rept. **286**, 53 (1997).
[2] L. Herrera, J. Ospino, and A. Di Prisco, Phys. Rev. D **77**, 027502 (2008), 0712.0713.
[3] L. Herrera, Phys. Rev. D **101**, 104024 (2020), 2005.06358.
[4] K. Schwarzschild, Sitzungsberichte der königlich preussischen Akademie der Wissenschaften pp. 189–196 (1916).
[5] P. S. Florides, Proceedings of the Royal Society of London. A. Mathematical and Physical Sciences **337**, 529 (1974).
[6] Ø. Grøn, General relativity and gravitation **18**, 591 (1986).
[7] K. Kohri, Phys. Rev. D **64**, 043515 (2001), astro-ph/0103411.
[8] L. Gabbanelli, J. Ovalle, A. Sotomayor, Z. Stuchlik, and R. Casadio, Eur. Phys. J. C **79**, 486 (2019), 1905.10162.
[9] C. Posada and C. Chirenti, Class. Quant. Grav. **36**, 065004 (2019), 1811.09589.
[10] X. Calmet, R. Casadio, and F. Kuipers, Phys. Rev. D **102**, 026018 (2020), 2007.05416.
[11] R. C. Tolman, Proc. Nat. Acad. Sci. **20**, 169 (1934).
[12] R. C. Tolman, Physical Review **55**, 364 (1939).
[13] J. R. Oppenheimer and G. M. Volkoff, Physical Review **55**, 374 (1939).
[14] C. E. Rhoades, Jr. and R. Ruffini, Phys. Rev. Lett. **32**, 324 (1974).
[15] S. Chandrasekhar and E. A. Milne, Mon. Not. Roy. Astron. Soc. **91**, 456 (1931).
[16] S. L. Shapiro and S. A. Teukolsky, *Black holes, white dwarfs and neutron stars. The physics of compact objects* (1983).
[17] J. E. Horvath, L. S. Rocha, A. Bernardo, R. Valentim, and M. G. B. de Avellar, Astron. Nachr. **342**, 294 (2021).
[18] B. Margalit and B. D. Metzger, Astrophys. J. Lett. **850**, L19 (2017), 1710.05938.
[19] M. Shibata, S. Fujibayashi, K. Hotokezaka, K. Kiuchi, K. Kyutoku, Y. Sekiguchi, and M. Tanaka, Phys. Rev. D **96**, 123012 (2017), 1710.07579.
[20] M. Ruiz, S. L. Shapiro, and A. Tsokaros, Phys. Rev. D **97**, 021501 (2018), 1711.00473.
[21] L. Rezzolla, E. R. Most, and L. R. Weih, Astrophys. J. Lett. **852**, L25 (2018), 1711.00314.
[22] H. T. Cromartie et al. (NANOGrav), Nature Astron. **4**, 72 (2019), 1904.06759.
[23] S. Nojiri and S. D. Odintsov, Phys. Rept. **505**, 59 (2011), 1011.0544.
[24] A. Joyce, B. Jain, J. Khoury, and M. Trodden, Phys. Rept. **568**, 1 (2015), 1407.0059.
[25] S. Nojiri, S. D. Odintsov, and V. K. Oikonomou, Phys. Rept. **692**, 1 (2017), 1705.11098.
[26] N. Frusciante and L. Perenon, Phys. Rept. **857**, 1 (2020), 1907.03150.
[27] G. J. Olmo, D. Rubiera-Garcia, and A. Wojnar, Physics Reports **876**, 1 (2020).
[28] F. S. N. Lobo, Phys. Rev. D **73**, 064028 (2006), gr-qc/0511003.
[29] F. Rahaman, S. Islam, P. K. F. Kuhfittig, and S. Ray, Phys. Rev. D **86**, 106010 (2012), 1209.2917.
[30] M. R. Mehdizadeh, M. Kord Zangeneh, and F. S. N. Lobo, Phys. Rev. D **91**, 084004 (2015), 1501.04773.
[31] M. Sharif and A. Ikram, Int. J. Mod. Phys. D **24**, 1550003 (2014).
[32] M. F. Shamir and M. Ahmad, Eur. Phys. J. C **77**, 674 (2017), 1705.06910.

- [33] B. Wu and C.-G. Huang, *Eur. Phys. J. C* **79**, 519 (2019), 1807.00683.
- [34] G. G. Nashed and S. Capozziello, *The European Physical Journal C* **80**, 1 (2020).
- [35] Z. Roupas and G. G. Nashed, *The European Physical Journal C* **80**, 1 (2020).
- [36] K. D. Krori and J. Barua, *Journal of Physics A* **8**, 508 (1975).
- [37] V. Varela, F. Rahaman, S. Ray, K. Chakraborty, and M. Kalam, *Phys. Rev. D* **82**, 044052 (2010), 1004.2165.
- [38] F. Rahaman, R. Sharma, S. Ray, R. Maulick, and I. Karar, *Eur. Phys. J. C* **72**, 2071 (2012), 1108.6125.
- [39] M. Kalam, F. Rahaman, S. Monowar Hossein, and S. Ray, *European Physical Journal C* **73**, 2409 (2013), 1301.0271.
- [40] P. Bhar, *Astrophys. Space Sci.* **356**, 365 (2015).
- [41] P. Bhar, *Astrophys. Space Sci.* **356**, 309 (2015), 1412.0107.
- [42] P. Bhar, F. Rahaman, A. Jawad, and S. Islam, *apss* **360**, 32 (2015).
- [43] G. Abbas, S. Qaisar, and A. Jawad, *apss* **359**, 17 (2015), 1509.06711.
- [44] M. Zubair, G. Abbas, and I. Noureen, *apss* **361**, 8 (2016), 1512.05202.
- [45] M. Zubair and G. Abbas, *apss* **361**, 342 (2016).
- [46] M. Ilyas, Z. Yousaf, M. Z. Bhatti, and B. Masud, *Astrophys. Space Sci.* **362**, 237 (2017).
- [47] Z. Yousaf, M. Z.-u.-H. Bhatti, and M. Ilyas, *Eur. Phys. J. C* **78**, 307 (2018), 1804.04953.
- [48] P. Saha and U. Debnath, *Eur. Phys. J. C* **79**, 919 (2019), 1911.10908.
- [49] G. G. L. Nashed, *Eur. Phys. J. C* **83**, 698 (2023), 2308.08565.
- [50] G. G. L. Nashed and W. El Hanafy, *JCAP* **09**, 038 (2023), 2306.13396.
- [51] G. G. L. Nashed, *Astrophys. J.* **950**, 129 (2023), 2306.10273.
- [52] G. G. L. Nashed and W. El Hanafy, *Eur. Phys. J. C* **82**, 679 (2022), 2208.13814.
- [53] G. G. L. Nashed, *Astrophys. J.* **919**, 113 (2021), 2108.04060.
- [54] I. Legred, K. Chatziioannou, R. Essick, S. Han, and P. Landry, *Phys. Rev. D* **104**, 063003 (2021), 2106.05313.
- [55] H. A. Buchdahl, *Physical Review* **116**, 1027 (1959).
- [56] B. V. Ivanov, *Physical Review D* **65**, 104011 (2002).
- [57] D. E. Barraco, V. H. Hamity, and R. J. Gleiser, *Physical Review D* **67**, 064003 (2003).
- [58] C. Böhmer and T. Harko, *Classical and Quantum Gravity* **23**, 6479 (2006).
- [59] Y. B. Zeldovich and I. D. Novikov, Chicago: University of Chicago Press (1971).
- [60] D. M. Podkowka, R. F. P. Mendes, and E. Poisson, *Phys. Rev. D* **98**, 064057 (2018), 1807.01565.
- [61] A. De Felice and S. Tsujikawa, *Living Rev. Rel.* **13**, 3 (2010), 1002.4928.
- [62] L. Herrera, *Phys. Lett. A* **165**, 206 (1992).
- [63] S. Chandrasekhar, *Astrophys. J.* **140**, 417 (1964), [Erratum: *Astrophys. J.* 140, 1342 (1964)].
- [64] R. Chan, L. Herrera, and N. Santos, *Monthly Notices of the Royal Astronomical Society* **265**, 533 (1993).
- [65] H. Heintzmann and W. Hillebrandt, *Astronomy and Astrophysics* **38**, 51 (1975).
- [66] H. Heiselberg and V. Pandharipande, *Ann. Rev. Nucl. Part. Sci.* **50**, 481 (2000), astro-ph/0003276.
- [67] J. M. Lattimer and M. Prakash, *Phys. Rept.* **442**, 109 (2007), astro-ph/0612440.
- [68] B. W. Lynn, A. E. Nelson, and N. Tetradis, *Nucl. Phys. B* **345**, 186 (1990).
- [69] R. C. Tolman, *Physical Review* **35**, 896 (1930).

